

Constraints on D'' structure using $PKP(AB-DF)$, $PKP(BC-DF)$ and $PcP-P$ traveltime data from broad-band records

Hrvoje Tkalčić*, Barbara Romanowicz and Nicolas Houy

Seismological Laboratory, University of California, Berkeley, 215, Mc Cone Hall, Berkeley, CA 94720, USA. E-mail: hrvoje@seismo.berkeley.edu

Accepted 2001 October 2. Received 2001 July 27; in original form 2000 January 8

SUMMARY

The effects of complex structure in the deep mantle and D'' on PKP differential traveltimes should be estimated accurately in order to reach reliable conclusions concerning the physical and chemical properties of the Earth's inner and outer core. In particular, it is important to assess how much of the data can be explained by mantle structure alone. For this purpose, we have assembled global data sets of high-quality $PKP(AB-DF)$, $PKP(BC-DF)$ and $PcP-P$ differential traveltimes measured on mostly broad-band records. The $PKP(AB-DF)$ data were inverted alone or jointly with $PcP-P$ data, to retrieve P -velocity maps of the lowermost 300 km of the mantle. Corrections for mantle structure above D'' were performed prior to inversion using recent tomographic models and the fit to the $PKP(BC-DF)$ data set was used to constrain damping in the inversions. We compare models obtained with and without polar PKP paths and find that their inclusion or exclusion does not significantly affect the resulting D'' model except under North America, where coverage is poor without polar paths. Our preferred model, obtained using $PKP(AB-DF)$ and $PcP-P$ data combined, explains over 80 per cent of the variance in $PKP(AB-DF)$, almost 60 per cent of the variance in $PcP-P$ and 27 per cent of the variance in $PKP(BC-DF)$ —a significant portion considering that the $PKP(BC-DF)$ data set was not used in the inversion. Our models are characterized by prominent fast features under mid-America and east Asia, a fast belt across the Pacific, a slow region under the southwestern Pacific and southern Africa, as well as sharp transitions from fast to slow, for instance under Alaska and the South Atlantic. The anomalous South Sandwich to Alaska data cannot fully be explained by D'' structure alone, unless very short-wavelength lateral variations are introduced. Models that allow for a modest level of constant transverse anisotropy in the inner core, compatible with normal mode splitting data, perform somewhat better, but still fail to explain the result of 2 s in $PKP(BC-DF)$ residuals, on these anomalous paths.

Key words: CMB, inner core anisotropy, PKP and $PcP-P$ traveltime, P -velocity structure in D'' , tomography.

1 INTRODUCTION

Over the last 15 years, numerous studies have documented the existence of lateral heterogeneity in D'' at many different scales. Global S -wave tomographic models indicate a significant increase in the rms velocity perturbations in the last 500 km of the mantle (e.g. Su *et al.* 1994; Masters *et al.* 1996; Li & Romanowicz 1996) and a change in the spectrum of heterogeneity, with a shift to low degrees. This is manifested by the now well-known pattern of large low-velocity 'plumes' in the central Pacific and under Africa, surrounded by a 'ring' of high velocities. While there is clear evidence

from these studies for the existence of a simple, long-wavelength pattern of heterogeneity in D'' , short-period studies of precursors to core phases indicate the presence of small-scale heterogeneity as well (e.g. Doornbos 1974; Haddon & Cleary 1974; Husebye *et al.* 1976; Bataille & Flatte 1988). More recent studies, based on observations of diffracted waves, have documented the existence of heterogeneity at intermediate scales (e.g. Wysession *et al.* 1992, 1995; Souriau & Poupinet 1994; Wysession 1996; Kuo 1999). Also, the amplitude of the lateral velocity variations has been shown to be larger by a factor of 2 to 3 than that found from tomographic studies (Ritsema *et al.* 1998; Bréger *et al.* 2000), with strong lateral gradients over distances of a few hundred kilometres (Bréger & Romanowicz 1998; Ni & Helmberger 2000). There is also evidence for the presence of extreme structures, such as ultralow P -velocity zones (Garnero & Helmberger 1995, 1996; Sylvander *et al.* 1997), which may require partial melting (e.g. Williams & Garnero 1996).

*Now at: Institute of Geophysics and Planetary Physics, Scripps Institute of Oceanography, University of California, San Diego, La Jolla, USA. E-mail: hrvoje@igpp.ucsd.edu

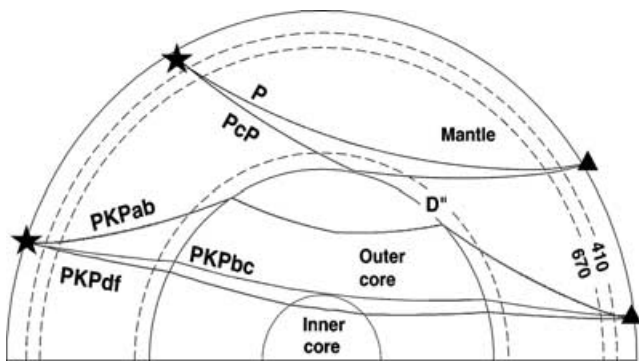


Figure 1. Cross-section of Earth showing the paths of P , PcP , $PKPab$, $PKPbc$ and $PKPab$ body waves.

While most studies of D'' use body waves turning in the mantle, the core phase $PKP(AB)$, which interacts with D'' at grazing incidence (Fig. 1), can also be used to investigate lateral heterogeneity at the base of the mantle. Attempts at such studies were pioneered by Sacks *et al.* (1979) and Snocke & Sacks (1986), who interpreted amplitude ratios of $PKP(AB)$ and $PKP(DF)$ in terms of heterogeneity in D'' . Sylvander & Souriau (1996) used $PKP(AB-BC)$ differential traveltimes to retrieve P -velocity structure in the lowermost 300 km of the mantle. More recently, Bréger *et al.* (2000) showed, in a forward modelling experiment, that realistic modifications to existing lowermost-mantle tomographic models could explain most of the trends in the observed $PKP(AB-DF)$ traveltime data, including variations with angle of the DF ray path, as measured at its bottom point, with respect to the axis of rotation of the Earth. These variations are generally interpreted in terms of simple models of anisotropy in the inner core, as first proposed by Morelli *et al.* (1986). Bréger *et al.* (2000) proposed that the observed trends were largely as a result of the interaction of unevenly distributed PKP paths with the strong gradients of structure at the border of the African plume. There have also been attempts to retrieve core-mantle topography using PKP phases, with little agreement in the results, most probably caused by trade-offs between core-mantle boundary (CMB) topography and heterogeneity in D'' combined with the noisy character of the ISC data set used (i.e. Creager & Jordan 1986; Morelli *et al.* 1986; Rodgers & Wahr 1993; Garcia & Souriau 2000).

There are two problems with using core phases to study D'' . First, the sampling of D'' achieved with the existing global data set is sparse, and makes it difficult to resolve the ambiguity in the location of the heterogeneity on the source or the station leg of $PKP(AB)$ in D'' . This can be remedied, to some extent, by using PKP data as a complement to other mantle sensitive data, such as P traveltimes, as has been done recently by Kárason & van der Hilst (2000). The second problem is that, by using $PKP(DF)$ as a reference phase, we introduce potential biases owing to inner-core anisotropy or heterogeneity. To avoid issues related to trade-offs between inner-core anisotropy and mantle structure, PKP data corresponding only to quasi-equatorial paths (waves travelling at large angles with respect to the Earth's rotation axis) are generally considered for the study of D'' structure.

In the present study, we analyse a global data set of carefully measured $PKP(AB-DF)$ traveltimes in an attempt to retrieve structure in the last 300 km of the mantle. We correct data for mantle structure using various existing P and S tomographic models, choosing the model that provides the best fits to our data sets. We complement the $PKP(AB-DF)$ data set with a global data set of hand-picked $PcP-P$ differential traveltimes to help resolve any ambiguity

in the location of heterogeneity on source or receiver sides. We have also collected a data set of hand-picked $PKP(BC-DF)$ traveltimes, which we use as constraints on the overall damping in our inversions. We compare models obtained using subsets of $PKP(AB-DF)$ traveltime data, in particular removing or including polar paths or the particularly anomalous paths corresponding to sources in the South Sandwich Islands and stations in Alaska, in order to assess what portion of the data set requires structure in the core. Finally, we also consider models in which we first correct the data for transverse isotropy in the inner core, at a level compatible with core mode splitting data.

2 DATA SETS AND DATA SELECTION

We use hand-picked $PKP(AB-DF)$, $PKP(BC-DF)$ and $PcP-P$ data sets of the highest quality, from a variety of sources. Using differential traveltime data reduces biases of mislocation in space and time, as well as unwanted effects imposed by source and receiver structure, owing to the proximity of the paths of the two rays in the crust and the upper mantle (e.g. Cormier & Choy 1986; Creager 1992) (Fig. 1). Any of these unwanted effects should have a similar influence on both rays, and thus can be significantly reduced.

$PKP(DF)$ is taken as the reference phase in this study, because the coverage of D'' available using $PKP(AB-BC)$ is much more limited owing to the narrow epicentral distance range at which $PKP(BC)$ is present. We therefore need to carefully consider possible effects of the inner core. On the other hand, it allows us to experiment regarding trade-offs between mantle and core structure.

$PKP(AB-DF)$ data set

Our own data set (subset 1) comprises differential traveltimes measured on vertical-component seismograms primarily from broadband digital stations, complemented by about 20 measurements from short-period records. Our data set represents an augmented version of that considered in Bréger *et al.* (2000) and referred to in Garnero (2000). Measurements are done by applying standard techniques, such as the Hilbert transform (Fig. 2a) followed by cross-correlation of $PKP(DF)$ and $PKP(AB)$ phases (Fig. 2b) in order to measure the precise time-shift between these two arrivals. In our experience, the best data come from large ($M_b > 6$) deep-focus earthquakes. However, we were able to make use of many shallow events with good signal-to-noise ratio. This involved identifying depth phases and comparing waveforms from several stations for the same event. We tried to process raw data without filtering whenever possible, and only in several instances do we bandpass-filter the broad-band waveforms between 0.5 and 2.0 Hz. The uncertainty in measurements is of the order of 0.1–0.2 s in most cases. However, difficulties in measurement sometimes arise when the shape of the Hilbert-transformed $PKP(AB)$ phase does not match that of $PKP(DF)$ very well, or when the first cycle of the $PKP(DF)$ waveform is unusually broad, which is probably associated with high attenuation in the inner core (e.g. Souriau & Romanowicz 1996). In such cases, the uncertainty in the measurement is about 0.5 s or larger, and such data were rejected following our low-tolerance approach.

In addition to measurement errors, we need to consider errors arising from source mislocation, even though we used relocated event parameters according to Engdahl *et al.* (1998). For instance, in $PKP(AB-DF)$ differential traveltimes, at epicentral distances of 150° and 175° , a 10 km error in the hypocentral location yields a differential time error of about 0.2 and 0.4 s, respectively. Similarly,

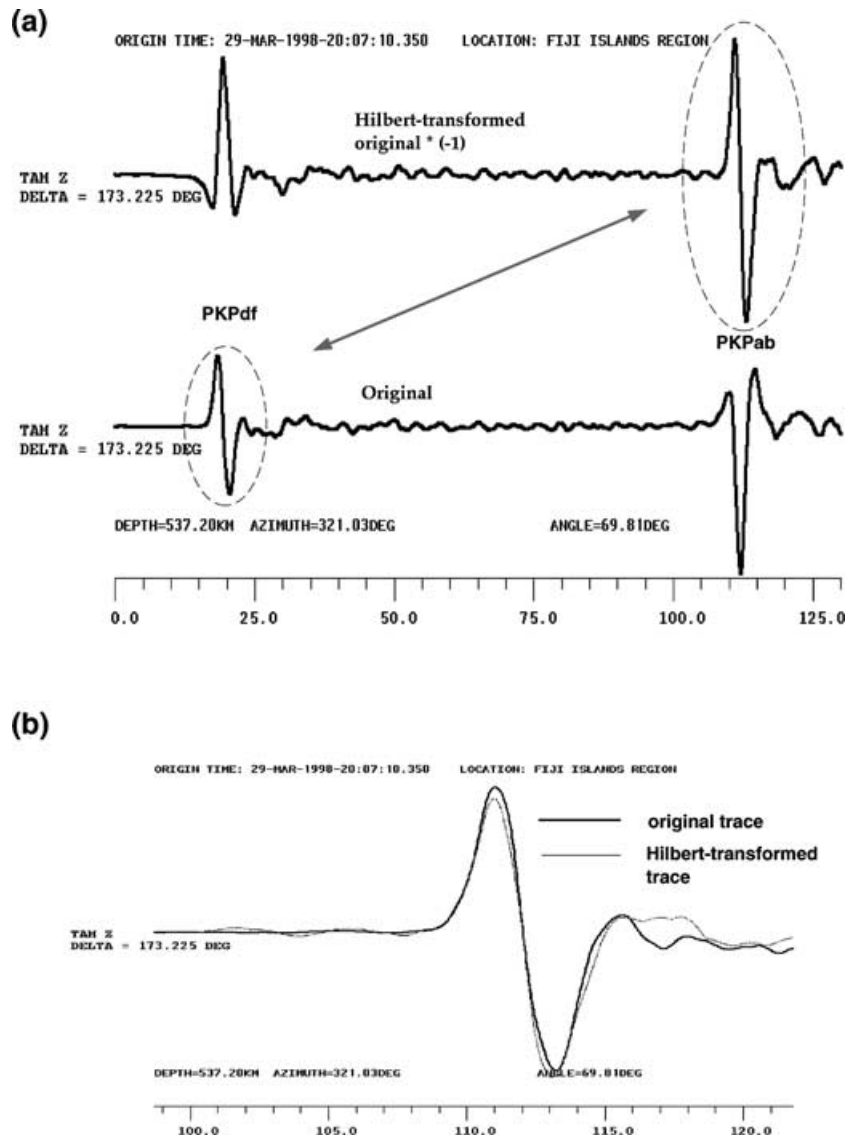


Figure 2. (a) Applying the Hilbert transform and changing the polarity of the *PKPab* phase produces a waveform similar to *PKPdf*; (b) overlapping the *PKPdf* waveform from the original trace and the *PKPab* waveform from the Hilbert-transformed trace, allows a measurement of the traveltime shift between them, with great accuracy.

at epicentral distances of 25° and 75° , a 10 km error in the hypocentral location would yield an error in *PcP*–*P* differential traveltimes of about 0.7 and 0.1 s, respectively. In summary, the total error in the differential residuals is estimated to be of the order of 0.5–1 s.

In order to obtain optimal sampling of D'' , we complemented our data set with three other existing subsets of hand-picked *PKP* data, from which all measurements qualified as ‘poor’ or worse were disregarded. Subset 2 comprises high-quality measurements from short-period instruments (McSweeney *et al.* 1997; Creager 1999). Subset 3 contains mostly data from broad-band instruments of the GEOSCOPE network (Souriau, personal communication). Finally, subset 4 comprises data derived from seismograms of a broad-band PASSCAL experiment in India (Wysession, personal communication). To avoid redundancy of measurements, we had to set some selective criteria. We used our own complete data set as a starting point, and added the largest one of the three remaining data sets (subset 2), removing the repetitive measurements from it. Then, we added subset 3 and finally subset 4, repeating the procedure of removing the repetitive measurements. This procedure only slightly reduced

the total number of measurements, since the four data sets are mutually complementary. The closer analysis of multiple measurements showed a great level of consistency among different seismogram-readers, which is not surprising, since we limited ourselves to only the highest-quality data. Furthermore, suspicious anomalous data were detected and rejected on the basis of cross-checking trends for individual stations and individual earthquake source regions.

Furthermore, in order to avoid too much emphasis on specific paths, we used the summary ray approach to reduce the number of data on oversampled paths. In particular, two events, one from the southern mid-Atlantic ridge (1990 April 30) and one located south of Africa (1993 March 29), were well recorded at the short-period Alaskan network and at short-period networks in California, respectively (McSweeney *et al.* 1997). An unusually good signal-to-noise ratio resulted in a couple of hundreds of picks, which we reduced to only about 20, by creating summary rays with respect to the epicentral distance and the azimuth. However, these measurements, along with others in Alaska, are of great importance in investigating

the short-scale deep-mantle heterogeneity as shown in Romanowicz *et al.* (2001).

The final data set comprises a total of 1329 high-quality *PKP*(AB–DF) differential traveltimes. We computed traveltime residuals with respect to the standard ak135 model (Kennett *et al.* 1995) accounting for Earth’s ellipticity (Kennett & Engdahl, personal communication), and after relocation according to Engdahl *et al.* (1998). The traveltime residuals from the different subsets considered (after declustering as mentioned above) are displayed in Fig. 3(a) as a function of angle with respect to the rotation axis of the Earth (this angle is hereafter called ξ). Fig. 3(a) shows that there could be two trends in the residuals. For angles of less than 35° , residuals are shifted toward higher values on average, although a large scatter at $\xi \approx 30^\circ$ is evident. All five residuals available for $\xi < 20^\circ$ are positive and greater than about 1.5 s. Taking a closer look at the traces from this group reveals that large residuals are mostly caused by advanced *PKP*(DF) arrivals with respect to the ak135 model that we use as a reference. Some specific paths are indicated on the same figure. The majority of the most anomalous data correspond to measurements obtained from the short-period Alaskan network from a single event on the South Atlantic mid-ocean ridge (1990 April 30, 54.28°S , 1.27°E), and measurements originating from events at the South Sandwich Islands recorded at station COL in Alaska and stations SEY, NRIL and BILL in northeast Asia. In addition, there is one very anomalous measurement corresponding to *PKP* arrivals from the northern hemisphere (Svalbard region), recorded at station SPA (South Pole).

It is clear that models of constant anisotropy throughout the inner core cannot explain such data scatter, in particular, the range of over 5 s at ξ about 30° . Between about 30° and 45° , residuals span over 7 s (from about +5 to –2 s). Adopting the definition of a quasi-eastern (longitude from $+43^\circ\text{E}$ to $+177^\circ\text{E}$) and a quasi-western hemisphere of Tanaka & Hamaguchi (1997) yields results that are in agreement with the work of these authors (Fig. 3b). Most of the largest residuals correspond to *PKP*(DF) turning in the quasi-western hemisphere. For the equatorial paths, the scatter is smaller for the quasi-eastern hemisphere, which is, on average, faster (e.g. Creager 1999). Furthermore, in the western hemisphere, except for the cluster of very anomalous paths around $\xi = 30^\circ$, very few data points are available to indicate the characteristic trend of progressively increasing anomaly for polar paths. In fact, all but one very polar path ($\xi < 20^\circ$, station SPA) have smaller residuals than the paths corresponding to slightly larger ξ .

PKP(BC–DF) data set

We have also assembled a high-quality *PKP*(BC–DF) data set, following the same selective criteria as in collecting *PKP*(AB–DF) data. This data set will not be used directly in the inversion, but rather to test how well the D'' model derived from *PKP*(AB–DF) and *PcP* data can explain the *PKP*(BC–DF) traveltime residuals. The advantage of *PKP*(BC–DF) is that the ray paths for the two branches are close together throughout the mantle, so that corrections for mantle structure (outside of D'') are less critical than for *PKP*(AB–DF). However, the sampling of D'' is rather poor for BC–DF. Also, the separation of the two phases is less than 400 km in D'' , so that BC–DF is best suited for studying short-scale heterogeneity at a regional scale, which is beyond the scope of our study. Testing the fit to *PKP*(BC–DF) of the D'' model obtained using *PKP*(AB–DF) and *PcP*–*P* can provide information on the scale of lateral heterogeneity in D'' , and on how much structure might be required in the core.

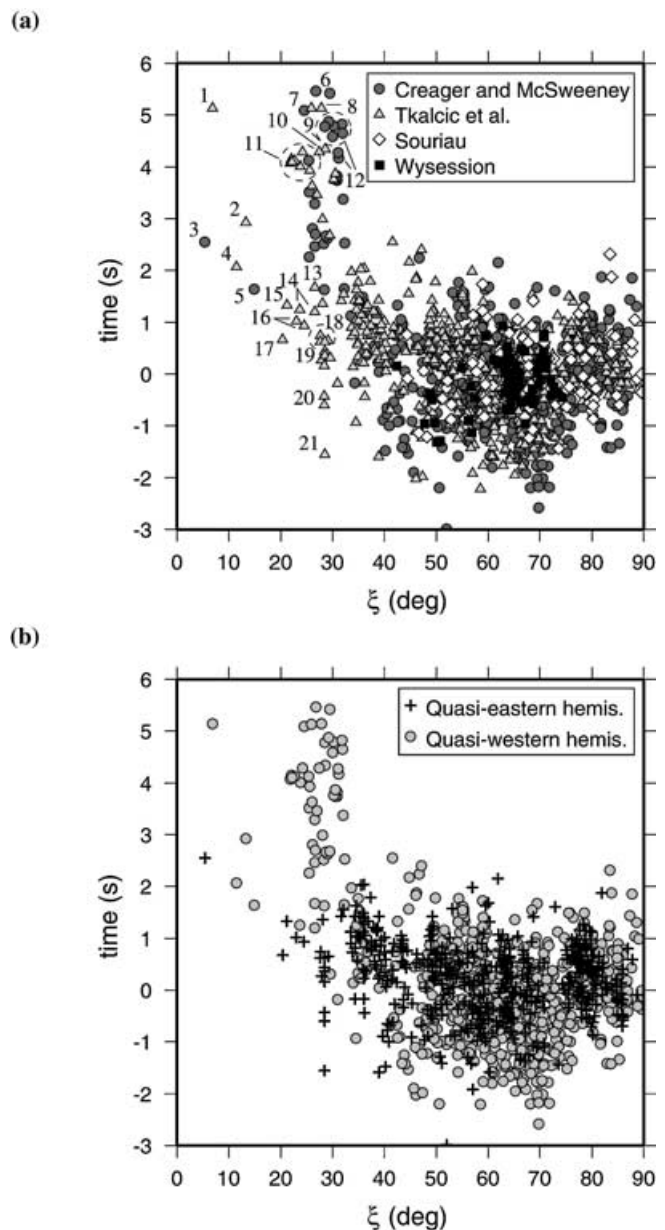


Figure 3. (a) The declustered subsets of *PKP*(AB–DF) differential traveltime residuals used in this study. Different symbols, corresponding to data from different analyses are explained in the legend. Residuals are calculated with respect to the ak135 model (Kennett *et al.* 1995) and plotted with respect to the angle ξ between the *PKP*(DF) leg in the inner core and the rotation axis of the Earth. Standard ellipticity corrections were applied. All earthquake locations and origin times are corrected with respect to the relocation catalogue of Engdahl *et al.* (1998). Some specific polar paths are indicated by numbers as follows: (1) Svalbard Sea to SPA; (2) 63°N , 143°W to SPA; (3) 79°N , 124°E to SPA; (4) 67°N , 173°W to SPA; (5) 60°N , 153°W to SPA; (6) mid-Atlantic ridge to Alaska; (7) South Sandwich Islands to COL; (8) South Sandwich Islands to BILL; (9) South Sandwich Islands to SEY; (10) southeast Pacific to NRIL; (11) South Sandwich Islands to COL and NRIL; (12) mid-Atlantic ridge to Alaska; (13) south of New Zealand to FRB; (14) Bouvet Islands to COLA and INK; (15) Aleutian Islands to SYO; (16) Sea of Okhotsk to SYO; (17) south of New Zealand to KBS; (18) various locations to SYO; (19), (20) and (21) Aleutian Islands to SYO. (b) Same as (a), where circles and pluses correspond to paths for which *PKP*(DF) bottoms out in the quasi-western and quasi-eastern hemisphere, respectively, as defined by Tanaka & Hamaguchi (1997).

The $PKP(BC-DF)$ data set used in this study also consists of four independent subsets. We used our own data set as a base, and added the largest one of the three remaining data sets (McSweeney *et al.* 1997; Creager 1999), removing the repetitive measurements from it. Then, we added subset 3 (Tanaka & Hamaguchi 1997) and subset 4 (Souriau, personal communication), repeating the procedure of reducing the repetitive measurements. The total number of data after declustering is 901. Traveltime residuals were calculated with respect to model ak135 and corrected for ellipticity, using relocated event coordinates from Engdahl *et al.* (1998). In addition, we declustered the $PKP(BC-DF)$ data set, following the same summary ray approach as described in the previous section on $PKP(AB-DF)$ data. $PKP(BC-DF)$ residuals from all four subsets are plotted in Fig. 4(a) as a function of ξ . Comparing with Fig. 3(a), it is clear that the scatter in equatorial $PKP(BC-DF)$ data is less pronounced than in $PKP(AB-DF)$ residuals. Residuals span roughly from 4.6 to -1.2 s and equatorial data are largely confined between ± 1 s (compared with ± 2 s for $AB-DF$). This is generally interpreted as being due to the fact that the paths of BC and DF are much closer than those of AB and DF in the mantle, particularly so in D'' .

In Fig. 4(b), we plotted the $PKP(BC-DF)$ data set with respect to ξ , distinguishing the two quasi-hemispheres, as defined above. The results confirm those of Tanaka & Hamaguchi (1997) (their Fig. 11) and Creager (1999) (his Fig. 2b, although his definition of hemispheres is somewhat different): the quasi-eastern hemisphere is faster on average, and does not show a strong trend of increasing residuals with decreasing angle ξ , in contrast to the quasi-western hemisphere. There are, however, other important observations: first, some very polar paths ($10^\circ < \xi < 20^\circ$) have smaller residuals than paths corresponding to larger ξ , just as was the case for $PKP(AB-DF)$. Second, for ξ between $\approx 20^\circ$ and 30° , the data can be fit rather well with a steep linear trend, spanning almost 5 s in traveltime anomaly (from $+4.6$ to -0.3 s).

Just as for $PKP(AB-DF)$, in order to fit the data in the western hemisphere with a constant transverse anisotropy model of the inner core as proposed by Creager (1992), one needs to exclude the South Sandwich/South Atlantic to Alaska paths. Since DF is the common phase in both data sets, the simplest explanation, as proposed by Creager (1999), is that the anomalous observations corresponding to these paths originate in the inner core. A recent analysis of Alaskan data indicates that this anomaly is sensed by both $PKP(DF)$ and $PKP(BC)$ and therefore must originate outside of the inner core (Romanowicz *et al.* 2001).

$PcP-P$ data set

To complement the $PKP(AB-DF)$ data set with independent data that can help resolve the source/station side ambiguity, we measured 1219 $PcP-P$ differential traveltimes. The compatibility of the data sets can be tested by comparing the models obtained using $PKP(AB-DF)$ data alone, versus using the joint data set.

In selecting our $PcP-P$ data set, we had to take into account the specific difficulties encountered with PcP measurements. PcP arrivals are very often buried in microseismic noise, especially for stations closer to the oceans. At epicentral distances larger than about 70° (depending on focal depth), they are buried in the P -wave coda. The $PcP-P$ measurements are also made more difficult by the interference of surface phases with PcP arrivals for shallow earthquakes. Again, we selected only high-quality vertical-component data from broad-band stations worldwide, assembling a unique global data set of hand-picked $PcP-P$ traveltime residuals in the distance range from about 25° to 75° .

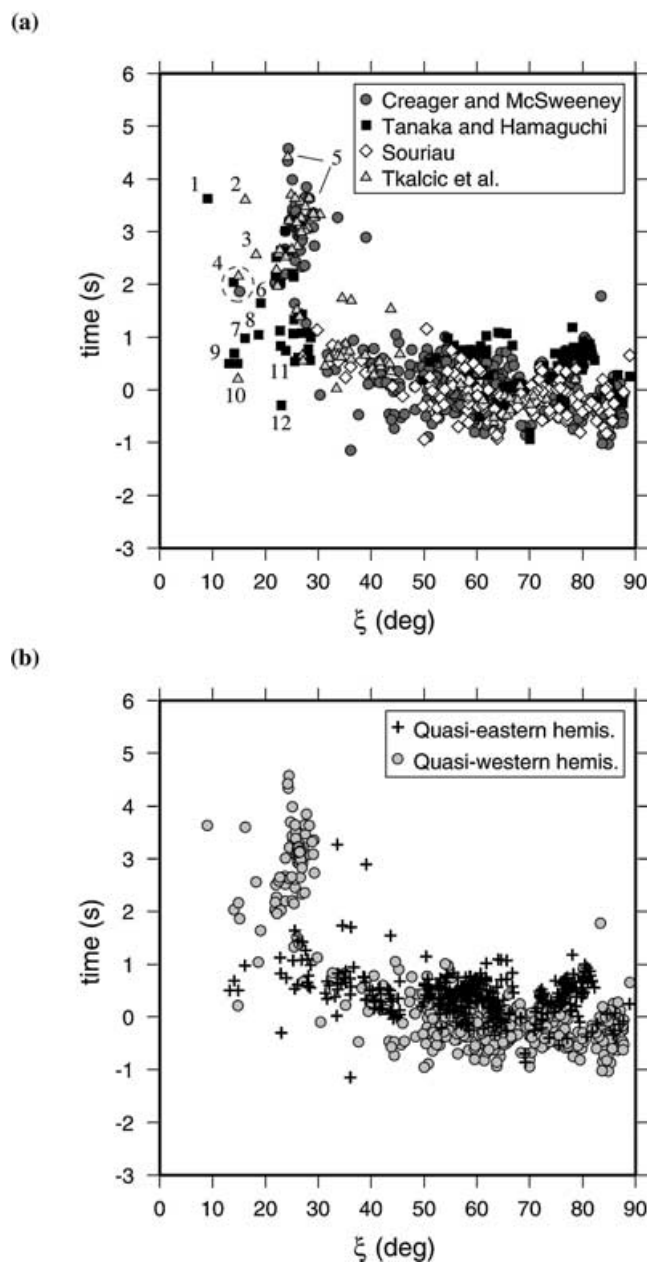


Figure 4. (a) The declustered subsets of $PKP(BC-DF)$ differential traveltime residuals used in this study. Different symbols, corresponding to data from different analysts are explained in the legend. Some specific polar paths are indicated by numbers as follows: (1) Novaya Zemlya to SNA; (2) Alaska to SPA; (3) South Sandwich Islands to MBC; (4) Alaska and north Canada to SPA; (5) South Sandwich Islands to northeast Asia and Alaska; (6) 52S, 140E to NOR; (7) Siber to SBA; (8) 53S, 160E to NOR; (9) 62N, 154E, 64N, 125E and 60N, 169E to SPA; (10) 60N, 153W to SPA; (11) various locations to SYO; (12) south of Australia to NOR. (b) Same as in (a), where now circles and pluses correspond to paths with $PKP(DF)$ bottoming in the quasi-western and quasi-eastern hemisphere, respectively.

The measurements are performed using the same waveform correlation methodology as described earlier for PKP . The residuals are computed with respect to the theoretical traveltimes from the ak135 model (Kennett *et al.* 1995), using relocated event coordinates (Engdahl *et al.* 1998), and corrected for ellipticity. Such calculated residuals vary in amplitude between -3 and 3 s. The residuals and coverage are shown in map form in Fig. 5.

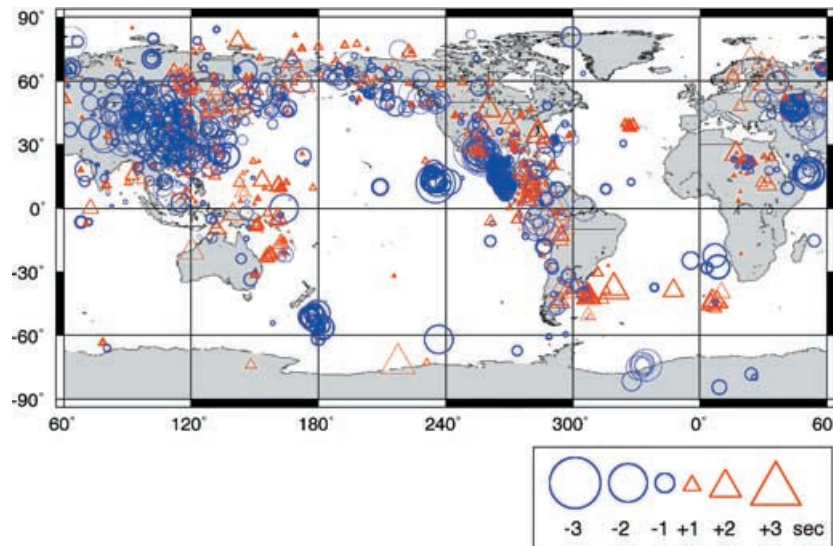


Figure 5. PcP - P traveltimes residuals plotted at the surface projections of PcP bouncing points. Triangles and circles indicate positive and negative residuals, respectively. The size of the symbol represents the value of the residual, the thickness of symbol lines scales with epicentral distance of the measurement: the thicker the line, the larger the epicentral distance. The largest symbols represent traveltimes anomaly of 2.8 s.

While the global coverage obtained with PcP - P is far from complete, in areas where there is good coverage we note a high level of spatial coherence in the data. An area of particular interest is middle America, where the alternation of positive and negative residuals indicates sharp lateral gradients on scalelengths of several hundred kilometres in the deep mantle, in agreement with recent results based on ScS - S data (Wysession *et al.* 2000).

3 CORRECTIONS FOR MANTLE STRUCTURE

Since we only invert for structure in the last 300 km of the mantle, to which the $PKP(AB-DF)$ data set is most sensitive, we need to take into account the possible contribution of overlying mantle heterogeneity. For this, we correct the observed residuals using predictions from available global tomographic mantle models. We select the model that provides the best variance reduction for our data set by systematically testing five P mantle tomographic models. We introduce a scaling factor h , to allow for the uncertainty in the amplitudes of lateral variations inherent to tomographic inversions. The scaling factor h is defined as $V_p(\text{new}) = hV_p(\text{orig})$, where $V_p(\text{orig})$ is the input tomographic model and $V_p(\text{new})$ is a virtual (scaled) model. A ‘good’ original P model should yield $h \approx 1$. If $h > 1$, the input model is overdamped, and if $h < 1$, it is either underdamped or, if combined with a small variance reduction, the distribution of heterogeneity may not be compatible with the PKP data set everywhere, so that the fitting procedure tends to minimize the contributions of the tomographic model.

For the purpose of the present study, we have calculated $PKP(AB-DF)$ traveltimes corrections for: (1) the whole mantle and (2) for the whole mantle without the lowermost 300 km thick layer. Paths from the same source region (sphere of radius $r = 100$ km) sampling the same block ($5^\circ \times 5^\circ$) at CMB were grouped and weighted prior to calculating variance reduction, according to criteria of similar sampling in the mantle. For instance, for the $PKP(AB-DF)$ quasi-equatorial subset, out of 1239 $PKP(AB-DF)$ ray pairs, we formed 610 bins with single rays, 126 bins with two rays and 82 bins with three or more rays.

Fig. 6(a) shows the variance reduction in the equatorial subset of $PKP(AB-DF)$ data ($\xi > 35^\circ$), plotted as a function of h , for

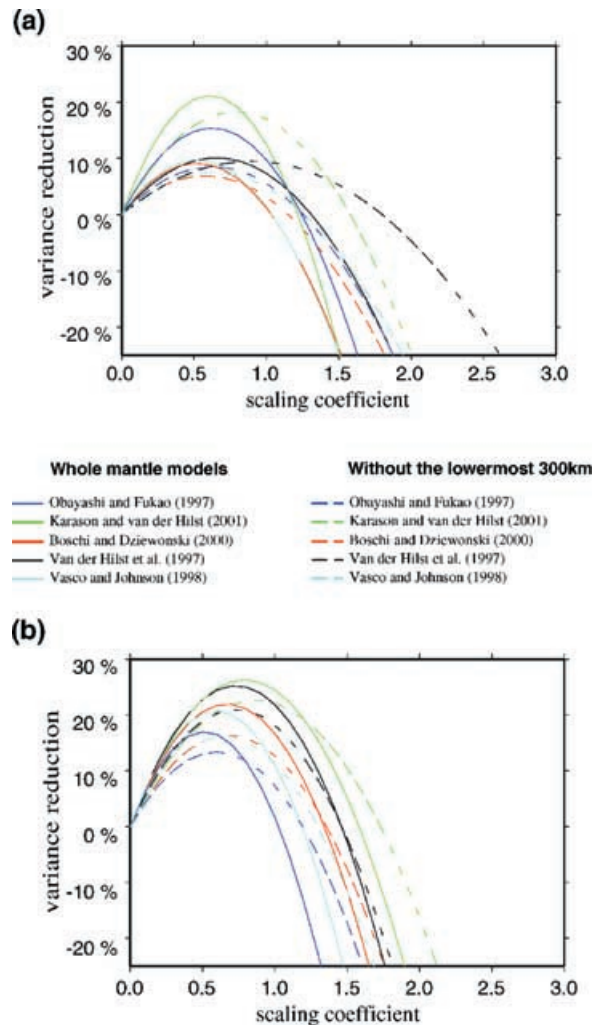


Figure 6. (a) Variance reduction in $PKP(AB-DF)$ data as a function of scaling coefficient h , as defined in text, for various P models, for the whole mantle (solid lines) and for the whole mantle stripped of D'' (dashed lines); (b) same as in (a), for the PcP - P data set.

five different global P -velocity mantle models (Obayashi & Fukao 1997; van der Hilst *et al.* 1997; Vasco & Johnson 1998; Boschi & Dziewonski 2000; Káráson & van der Hilst 2001). The model that gives the best variance reduction is that of Káráson & van der Hilst (2001), hereafter called KH2001 for the whole mantle, and KH2001m for the mantle stripped of the lowermost 300 km. For this model (as for others too), the best-fitting h is less than 1. It is closest to 1 when the bottom layer of the mantle is excluded, although in that case, the variance reduction is smaller. We infer tentatively that the detailed distribution of heterogeneity predicted by the tomographic P models is not perfectly compatible with the PKP data, particularly in D'' , or that, possibly, all the P models are underdamped.

We repeated the same experiment for the PcP - P data set, which is not affected by structure in the core, and furthermore, none of these data have been used in the construction of the tomographic models being tested. Interestingly, the KH2001 model also gives the best variance reduction in this case, of a similar amplitude (Fig. 6b). This indicates that the choice of the KH2001 model does not reflect a circular argument, as one might assume, given that some of the $PKP(AB-DF)$ data (measured by McSweeney *et al.* 1997; Creager 1999) were used in the construction of KH2001. The experiment with PcP - P gives somewhat larger scaling coefficients than for $PKP(AB-DF)$, close to 1 for the model stripped of the last 300 km of the mantle (KH2001m), indicating that overdamping is not the main factor leading to scaling factors smaller than 1, when $PKP(AB-DF)$ data are used. Rather, there is indeed some distribution of heterogeneity sampled by the $PKP(AB-DF)$ data set that is not present in KH2001. Thus, although the best-fitting model for $PKP(AB-DF)$ is for $h < 1$, we prefer to use the original model ($h = 1$) to correct residuals for mantle structure.

Relatively low percentages of variance reduction in both data sets open the question of how well modelled the lowermost-mantle layer is, in tomographic models. Our analysis shows that it is reasonable to assume that present mantle models can account for about 20–25 per cent of the variance in equatorial $PKP(AB-DF)$ differential traveltime data. The P -velocity model KH2001m is our preferred model for correcting both $PKP(AB-DF)$ and (PcP - P) traveltimes owing to larger variance reduction in comparison with other P models. Various S models (Grand *et al.* 1997; Masters *et al.* 1999; Gu & Dziewonski 2000; Mégnin & Romanowicz 2000) have also been tested with depth-dependent scaling factors (Tkalčić & Romanowicz 2000), however, they yield a smaller variance reduction in both PKP and PcP data sets, possibly indicating a lack of systematic correlation between P - and S -velocity heterogeneity in D'' (e.g. Wysession *et al.* 1992).

Recently, Bréger *et al.* (2000), showed by forward modelling that the trend in $PKP(AB-DF)$ residuals with respect to the angle ξ can be explained to a large extent by structure in D'' . According to another study (Creager 1999), polar $PKP(AB-DF)$ data show no correlation with the predictions from mantle models, concluding that there appears to be no significant contamination of the anisotropy signal by mantle structure. By using the model KH2001, we calculated correlation coefficients between mantle predictions and the $PKP(AB-DF)$ residuals, for the case of the complete data set and for the case of equatorial and polar subsets only (by using an arbitrary angle $\xi = 35^\circ$ to separate the two subsets of data). The results are shown in Table 1.

Correlation coefficients between observations and predictions are relatively high for both PKP and PcP data, especially for the polar subset. This is expected for PKP , since KH2001 is constructed by

Table 1. Variance reductions and correlation coefficients between observed and predicted subsets of data used in this study (after weighting was applied on the paths with similar geometry through the mantle). First and second columns refer to the whole mantle model by Káráson & van der Hilst (2000), referred as KH2001 in the text, while third and fourth columns refer to the same model stripped of the lowermost 300 km (KH2001m).

Test of KH2001 model	Whole mantle		Mantle stripped of the lowermost 300 km	
	Variance reduction (per cent)	Correlation coefficient	Variance reduction (per cent)	Correlation coefficient
Complete PKP(AB-DF) dataset	25.4	0.65	20.8	0.67
Equatorial PKP(AB-DF) subset	12.4	0.59	17.0	0.56
Polar PKP(AB-DF) subset	36.8	0.84	23.9	0.82
PcP - P dataset	31.3	0.55	29.6	0.54

including some manually picked PKP data, although previously corrected for inner-core anisotropy. Furthermore, variance reductions are best for the polar PKP data set, which could indicate a contribution of mantle structure to the trends seen in the polar paths. When we exclude the lowermost 300 km of the mantle, variance reduction for polar PKP subset drops significantly, while it increases in the case of the equatorial subset.

Since PcP - P may be more sensitive to mantle structure above D'' than $PKP(AB-DF)$, we have investigated whether it makes sense to attribute the observed variations in PcP - P traveltimes to structure in D'' . Fig. 7 shows the average relative velocity anomaly in D'' required to explain PcP - P residuals, as a function of the length of the PcP path in the lowermost 300 km of the mantle. The data have been corrected for the mantle above D'' using the KH2001m model. The length of path in D'' increases with epicentral distance, while the phases PcP and P have increasingly similar paths in the mantle. The range 700–1600 km corresponds to the epicentral distance range 30° – 75° .

If the tomographic model used to correct for the effects of the rest of the mantle is sufficiently accurate, Fig. 7 shows that, because of decreasing residuals with distance, to first order, the scale-length of heterogeneity that contributes to the observed residuals

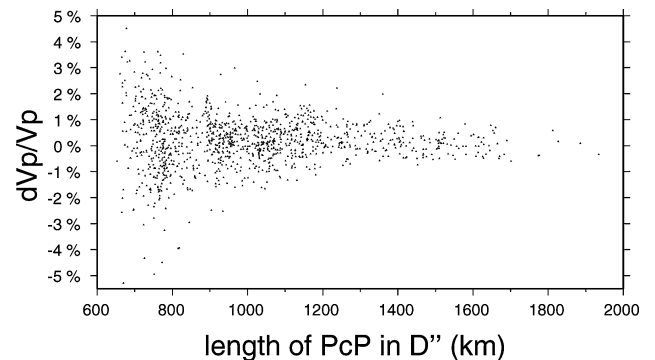


Figure 7. Average relative velocity variations in the lowermost 300 km of the mantle needed to explain PcP - P residuals, as a function of the length of PcP leg in the same layer. Mantle corrections are taken into account (from Káráson & van der Hilst 2000).

must be less than about 1000 km, which is in agreement with the lateral variations seen in Fig. 5. Because the residuals are organized symmetrically around the mean, we also infer that there are as many domains of faster than average velocities and of slower than average velocities. Thus, if there are domains of ultralow-velocity zones (e.g. Garnero *et al.* 1998), there must also be zones of very high velocity, in agreement with a recent suggestion based on observations of *ScP* waveforms (Castle & van der Hilst 2000). On the other hand, if model KH2001m does not adequately account for structure above *D''*, the trends observed in Fig. 7 could be at least partly explained by the decreasing separation between the two phases as the distance increases.

4 INVERSION

Global sampling and parametrization

Fig. 8 shows the distribution of surface projections of *PKP*(AB) and *PKP*(DF) legs sampling the lowermost 300 km of the mantle. It is clear from this figure, that the *D''* region is sampled well locally by *PKP*(AB) paths associated with earthquakes in the circum-pacific belt. The global coverage is limited not only by uneven global distribution of earthquakes, but also by the fact that differential traveltime measurements can be performed only for stations that are located between about 150° and 180° in epicentral distance. In particular, regions beneath the mid-Pacific and Africa are not very well sampled. If the *D''* region is parametrized by equiangular 5° × 5° block cells, it can be seen from Fig. 9(a) that the best sampled regions are located beneath South America, Caribbean Sea, southwestern Atlantic, Asia, southwestern Pacific and Australia. The number of

hits per block in some areas, e.g. the South Sandwich Islands, exceeds 100. Better sampling in certain regions does not increase the reliability of the inversion results proportionally in the same regions, as it is very important to have crossing paths coming from different azimuths, in particular because of the problem of trade-off between the source and the receiver side of *D''*. An example of such a potential resolution problem is for the numerous paths stretching from the South Sandwich Island region to North America for which there are not many crossing paths in North America. A comparison between Figs 5 and 8 shows that inclusion of *PcP*–*P* data helps to improve sampling in Asia, mid-America and Africa, and should help resolve source–receiver ambiguity in *PKP* on the paths between South Atlantic and Asia.

Although somewhat arbitrary, we use 300 km as a thickness for the *D''* layer, bearing in mind that fixed thickness trades off with the size of heterogeneity. We use two types of cell parametrization in this layer. In the first case, the layer is divided into a regular equiangular block grid with blocks of size 5° × 5° (Fig. 9a). At the CMB depth at the equator, this is about 300 × 300 km² which is comparable to the layer thickness. In the second case, the layer is divided into a variable-size block grid (Fig. 9b). We devised a scheme to define the variable-size blocks based on sampling. Each block should have at least three hits and we increase the size of the block by coalescing neighbouring blocks until the minimum hit count is reached. The largest cell size is set to be 10° × 10°. If a cell shape with a number of counts ≥ 3 cannot be found, then that region is rejected and excluded from inversion (white areas in Fig. 9b). Our algorithm produces a more uniform geographical distribution of counts and the ‘allowed’ shapes are chosen in such a way that the final grid does not consist of excessively elongated

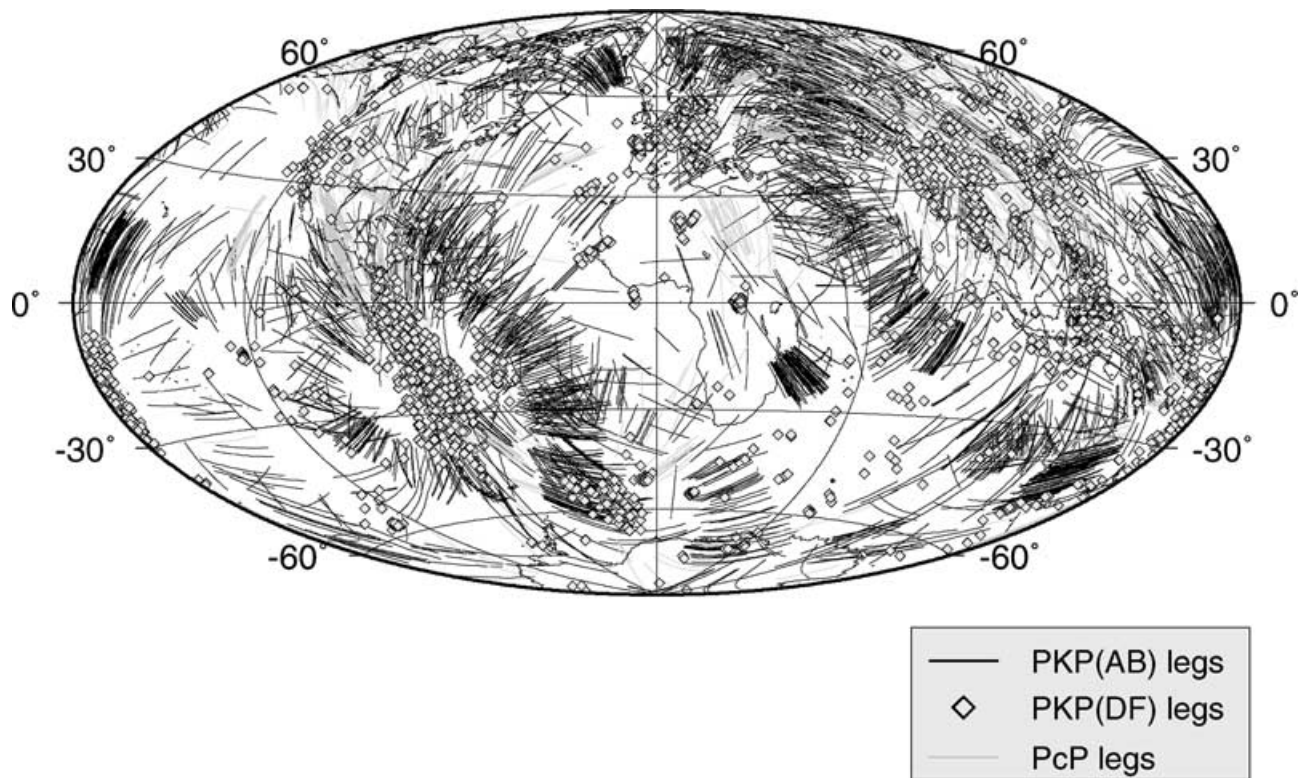


Figure 8. Surface projections of *PKP*(AB) and *PcP* legs sampling the lowermost 300 km of the mantle. Diamonds represent penetration points of *PKP*(DF) into the core (their legs sampling the lowermost 300 km of the mantle would project as points since they traverse that layer at almost vertical incidence).

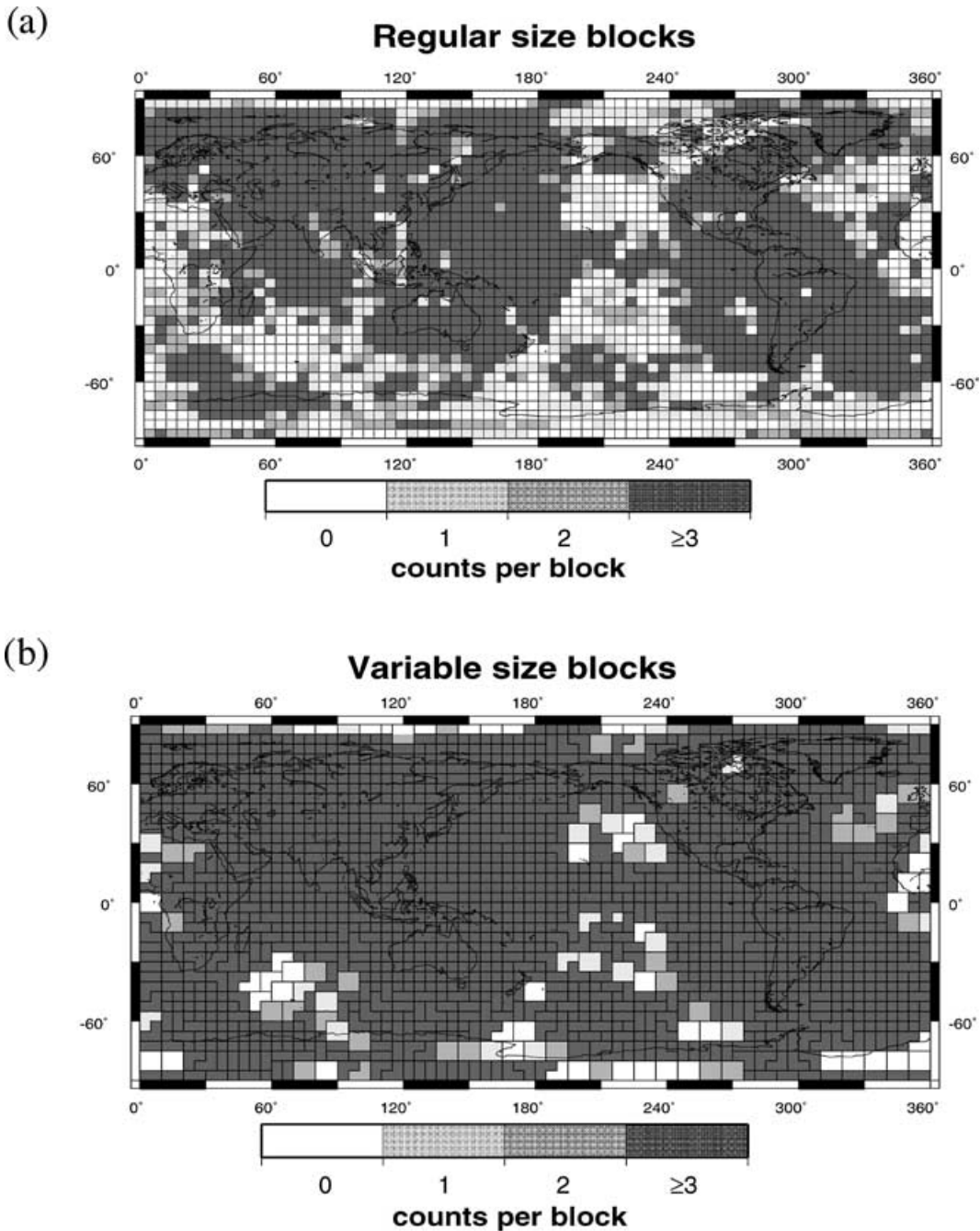


Figure 9. The sampling of D'' in terms of number of counts per block (number of rays crossing each particular block: (a) before the variable-size block algorithm is applied; (b) after the variable-size block algorithm is applied. The critical number of counts per block is set to be three in this example. White areas represent blocks that have been rejected because of insufficient sampling. Note that in (b), blocks have changed shape and increased their size in areas of poor sampling and remain small in well-sampled areas.

shapes, but rather ones with aspect ratio close to 1 (in contrast to Bijwaard *et al.* 1998). This technique allows us to preserve relatively small-sized blocks in regions with good coverage, while at the same time increasing the size in unsampled regions (compare Figs 9a and b).

Linear inversion is done by using lower triangular–upper triangular (LU) decomposition algorithm (Press *et al.* 1988), and by adding various damping factors to diagonal elements. We did not use any smoothness criteria, as several studies have documented strong lat-

eral gradients of structure in D'' and we wish to preserve those. The blocks that are not sampled are omitted, thus reducing the number of columns in the matrix. The variable size block approach ensures that the models obtained will not be strongly contaminated by the effects of undersampling.

In Fig. 10, we show an example of a resolution test. We constructed a synthetic model with a checkerboard pattern in D'' (a single layer), with the same size of heterogeneities as the size of the grid used in parametrization of our models (Fig. 10a), and no

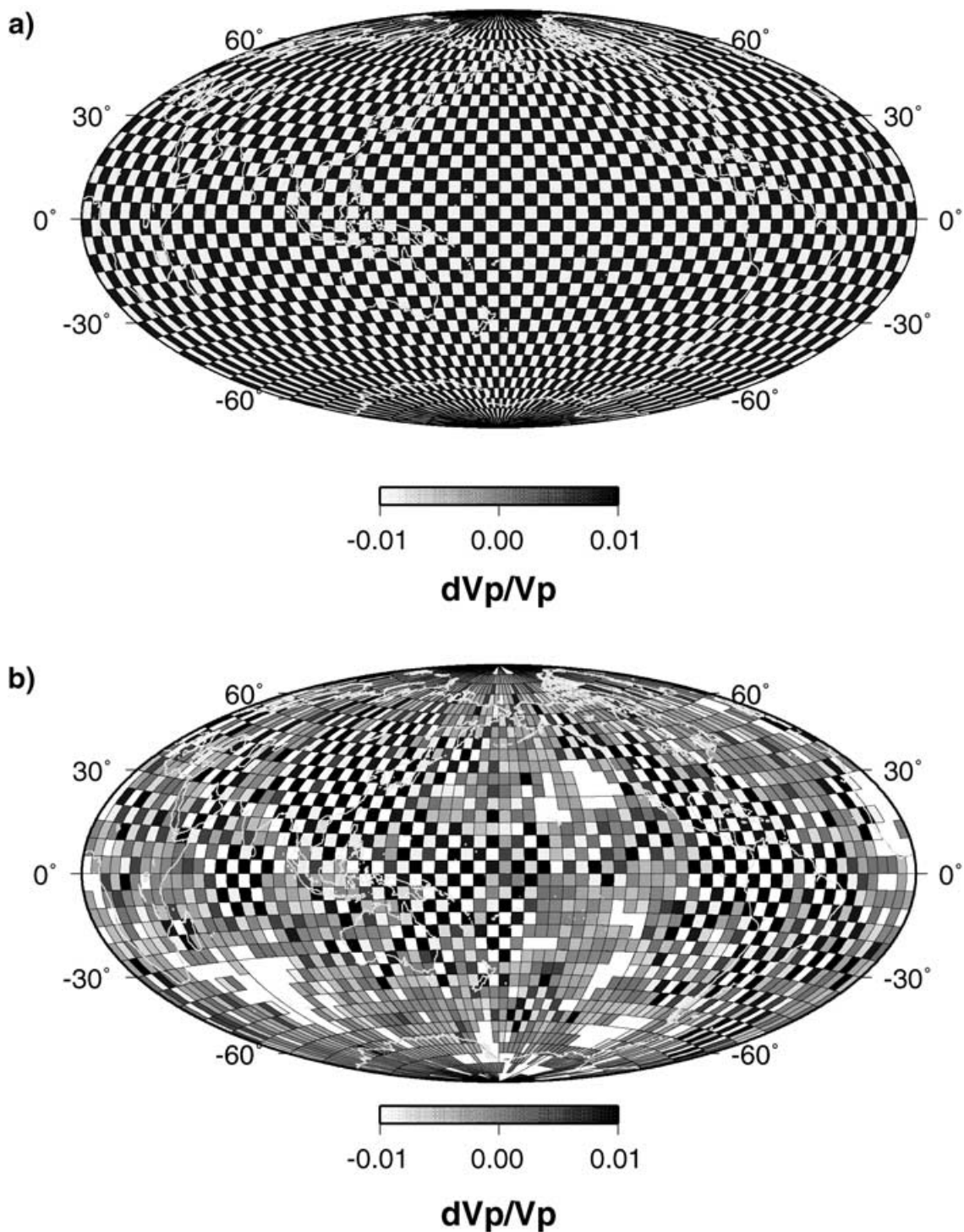


Figure 10. (a) The synthetic checker-board input model, parametrized in terms of equiangular cells of size $5^\circ \times 5^\circ$ (same as in inversion); (b) the corresponding output model, for the optimal damping. White non-gridded areas are non-sampled blocks.

structure in the core. The output model for the optimal damping (as discussed below) and the entire *PKP*(AB–DF) and *PcP*–*P* data set is shown in Fig. 10(b). The comparison with Fig. 7 confirms that the best results are obtained in well-covered regions (note that the projection in Fig. 8 is centred on Africa in order to emphasize the polar paths from South Atlantic to Alaska, while the projection in Fig. 10 is centred on the Pacific). Non-sampled blocks are shown as white, non-gridded areas.

5 DISCUSSION OF RESULTING MODELS

We have derived a series of models of *P*-velocity anomalies in D' using different subsets of data, in order to investigate the effect of including or excluding polar/anomalous paths in the inversion, the constraints provided by the *PcP*–*P* data set, and the effects of accounting for simple inner-core anisotropy structure. The resulting

Table 2. Description of models and data sets used in their construction. It is also indicated which corrections are applied to data before the inversion.

Model	Data description
TRH_K	Data: complete PKP(AB-DF) dataset. Corrected for: KH2001m before inversion
TRH_Keq	Data: ‘Equatorial’ subset of PKP (AB-DF) (paths with $\zeta > 35^\circ$). Corrected for: KH2001m before inversion
TRH_Knsa	Data: PKP (AB-DF) without subset of paths from south Atlantic to Alaska. Corrected for: KH2001m before inversion
TRH_KC	Data: complete PKP (AB-DF) dataset + PcP-P dataset. Corrected for: KH2001m before inversion
TRH_KCeq	Data: ‘Equatorial’ subset of PKP (AB-DF) (paths with $\zeta > 35^\circ$) + PcP-P dataset. Corrected for: KH2001m before inversion
TRH_KCnsa	Data: PKP (AB-DF) without subset of paths from south Atlantic to Alaska + PcP-P dataset. Corrected for: KH2001m before inversion
TRH_KCa	Data: complete PKP (AB-DF) dataset + PcP-P dataset. Corrected for: KH2001m and TR95 before inversion

models are labelled according to a scheme described in Table 2 for the models without and with inner-core anisotropy, respectively. In both cases, we have considered inversions with three different subsets of PKP data:

- (1) the entire data set;
- (2) excluding quasi-polar data (angles $\xi < 40^\circ$);
- (3) excluding anomalous paths between the South Atlantic and Alaska, but including other quasi-polar paths.

Prior to inversion, we corrected PKP(AB-DF) and PcP-P data for mantle structure above D'' , using model KH2001m. In the series of inversions ‘with’ inner-core anisotropy, we also corrected the PKP(AB-DF) residuals for the particular inner-core anisotropy model considered. We tried several recent models (Creager 1992; Durek & Romanowicz 1999; Tromp 1993, 1995).

In order to constrain the choice of damping in the inversions, we compute the fit to the PKP(BC-DF) data set and keep the model that provides the best fit to this data set. This will be discussed more extensively below.

The models derived using only PKP(AB-DF) data are not shown, for the sake of space. They are quite compatible with the models obtained using both PKP(AB-DF) and PcP-P, as can be assessed from the correlation coefficients shown in Table 3, except under southeastern Asia, where structure could not be well resolved with PKP(AB-DF) data alone (caused by source–station ambiguity, which is resolved by the inclusion of PcP-P data). Since the joint PKP/PcP inversions correspond to better sampling of D'' , we concentrate on discussing those.

The models obtained using the complete PKP(AB-DF) data set are shown in Fig. 11. Prior to plotting the models, we smoothed them using a 3×3 blocks moving-average scheme and removed the mean. For the models with inner-core anisotropy, the best fit to PKP(BC-DF) is obtained when correcting for the radially dependent model of inner-core anisotropy derived to fit both normal mode and traveltime data (Tromp 1995). We further refer to this model as TR95. The resulting D'' model, labelled as TRH_KCa, is shown in Fig. 11(b).

The correlation coefficient between models TRH_KCa and TRH_KC (Fig. 11, Table 3) is 0.71. Although amplitudes of P -velocity anomalies in TRH_KCa are weaker (note the change in colour palette), the distributions of anomalies in D'' are very similar. Both models show prominent fast features in eastern Asia, Arabian Sea, South Atlantic, Caribbean Sea and Alaska, as well as slow features in the southwest Pacific and under southern Africa. There is a horizontal band of fast velocities across the North Pacific, which is in agreement with some P models derived from ISC data (e.g. Obayashi & Fukao 1997; Vasco & Johnson 1998; Boschi & Dziewonski 2000). Slow anomalies are observed under North America (somewhat stronger in model TRH_KC) which is not consistent with most P models derived from ISC data (e.g. Obayashi & Fukao 1997; Vasco & Johnson 1998; Boschi & Dziewonski 2000; Káráson & van der Hilst 2000), but is consistent with the results of Sylvander & Souriau (1996b) and the S -velocity model of Masters *et al.* (1999).

In general, TRH_KCa does not differ much from TRH_KC, except south of Africa where TRH_KC has negative and TRH_KCa positive anomalies. Sharp transitions from fast to slow in the southern Atlantic, as well as in central America are present in both models. We will discuss the fits to the PKP(BC-DF) data extensively below.

In Fig. 12, we further consider the influence of anomalous/polar paths on the inversions in which we do not correct data for inner-core anisotropy. The models are shown here in a different, polar projection, emphasizing the regions that might be most affected by the inclusion or exclusion of polar paths. Model TRH_KC, which includes all data, is shown again in Fig. 12(a), while Figs 12(b) and (c) show models TRH_KCeq (no equatorial paths) and TRH_KCnsa (no South Atlantic to Alaska paths), respectively, as defined in Table 2.

All three models show generally good agreement, as can also be assessed from Table 3, which shows that correlation coefficients are between 0.76 and 0.93 for these models. When polar paths, which might be significantly affected by inner-core anisotropy, are excluded (model TRH_KCeq, Fig. 12b), the coverage of D'' decreases significantly under North America and the Atlantic Ocean. However, faster regions in the South Atlantic and mid-America remain stable after removal of the polar paths. The only prominent difference between this and the TRH_KC model (Fig. 12a) is the slow region beneath North America, which is not sampled by

Table 3. Correlation coefficient between various combinations of one-layered models of D'' obtained in this study.

Correlation coefficient	TRH_K	TRH_Keq	TRH_Knsa	TRH_KC	TRH_KCeq	TRH_KCnsa	TRH_KCa
TRH_K	1.00	0.65	0.89	0.83	0.47	0.71	0.58
TRH_Keq	0.65	1.00	0.76	0.52	0.68	0.57	0.50
TRH_Knsa	0.89	0.76	1.00	0.77	0.56	0.81	0.55
TRH_KC	0.83	0.52	0.77	1.00	0.76	0.93	0.71
TRH_KCeq	0.47	0.68	0.56	0.76	1.00	0.83	0.68
TRH_KCnsa	0.71	0.57	0.81	0.93	0.83	1.00	0.68
TRH_KCa	0.58	0.50	0.55	0.71	0.68	0.68	1.00

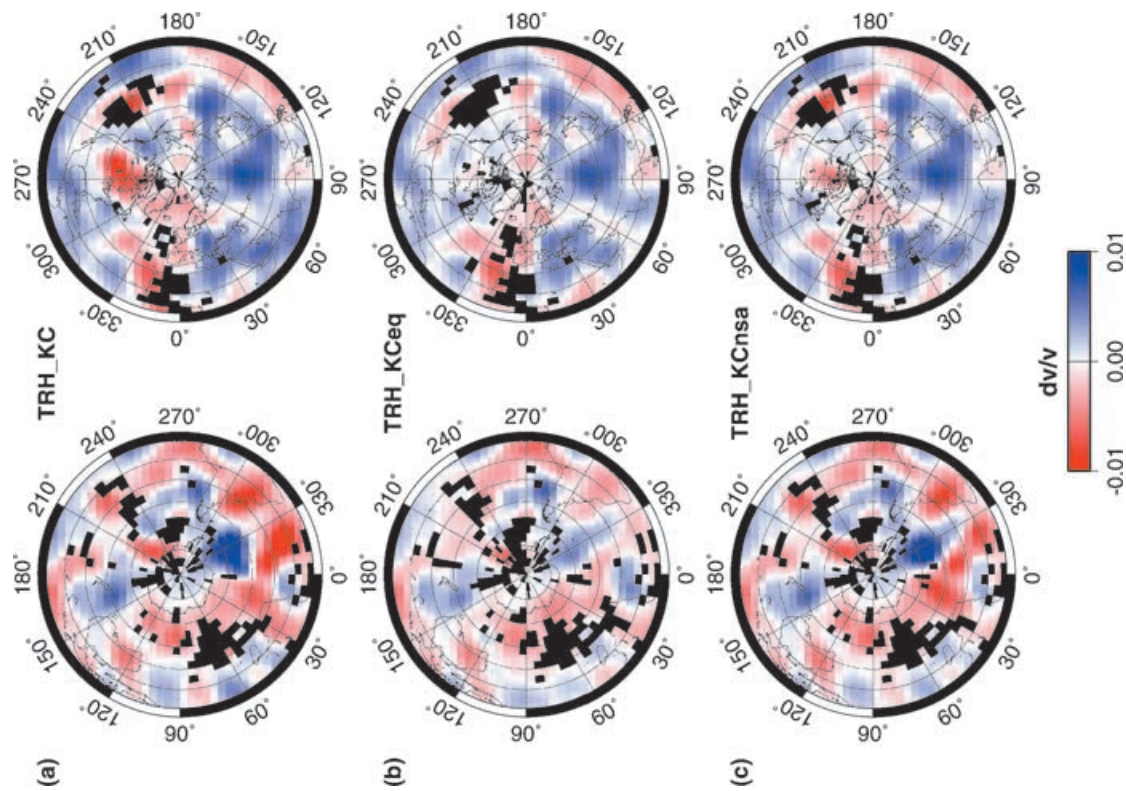


Figure 11. Models (a) TRH_KC and (b) TRH_KCa, for the optimal damping. These one-layered models represent P -velocity perturbations with respect to model ak135 (Kennett *et al.* 1995) in the bottom 300 km of the mantle. TRH_KC was obtained by inverting PKP (AB-DF) and PcP - P data simultaneously, without inner-core anisotropy. For TRH_KCa, the same data set was inverted, but first corrected for the transverse isotropy model of Tromp (1995). Blackened areas represent non-sampled regions.

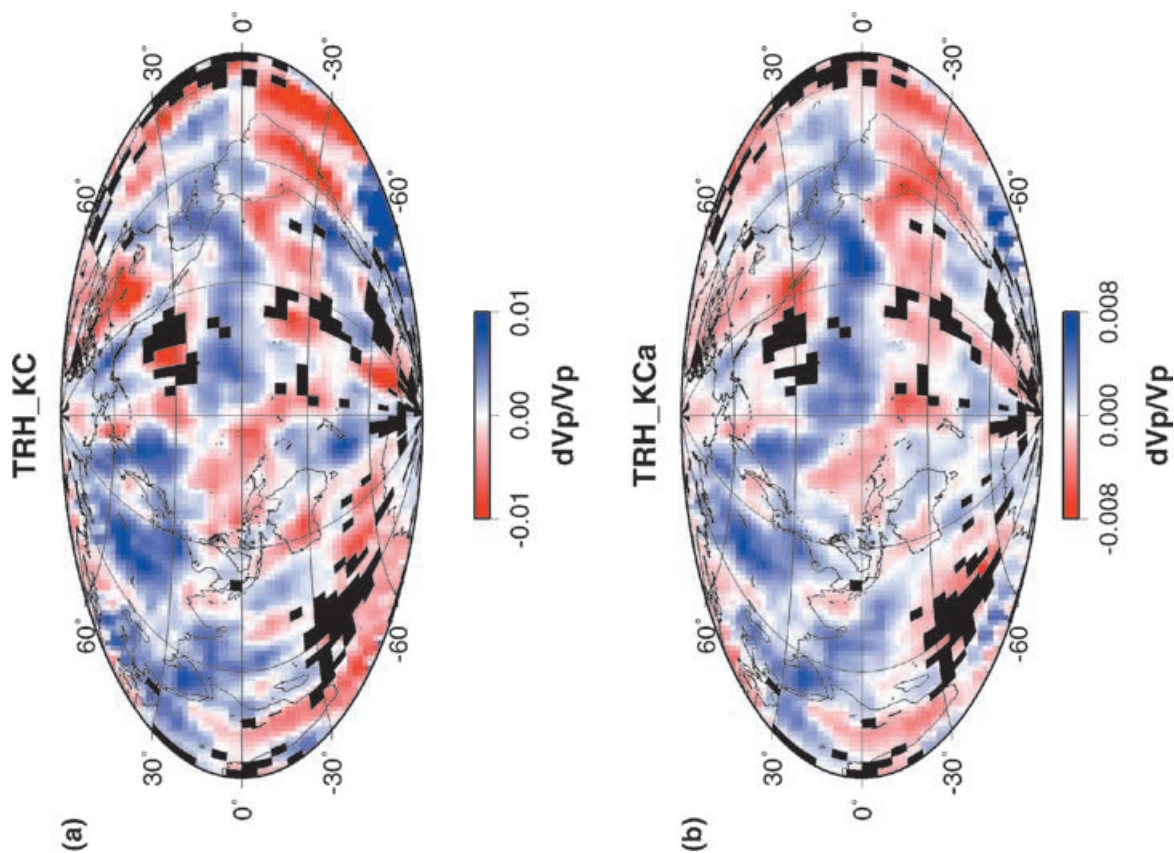


Figure 12. One layer models of P -wave velocity perturbations in the lowermost 300 km of the mantle, obtained from different combinations of data, as described in Table 2: (a) TRH_KC; (b) TRH_KCeq; (c) TRH_KCnsa. The models are shown here in polar projections centred on the South Pole (left) and North Pole (right).

equatorial paths only. However, we saw in Fig. 11 that this region remains mostly slow even when anisotropy is accounted for.

Although the number of hits per block under some parts of North America exceeds 10, there is not a substantial number of mutually crossing paths (Fig. 8). The reason for this is that there are numerous stations, but fewer useful earthquakes in that region. Most of the data that account for coverage under North America come from sources in the South Atlantic, in particular from the South Sandwich Islands region, and they are recorded by the Alaskan network. Hence, we could be mapping anomalies from the source side on to the receiver side of D'' . This could be addressed with some PcP data in North America. Unfortunately, at the moment there are not enough such data, mainly owing to the lack of earthquakes which would produce PcP waves that sample the D'' under North America. We considered this problem by removing all PKP paths from the South Atlantic to Alaska (a total of 90 paths after declustering) and performed the inversion for the remaining data set (including polar paths). The model we obtain in this way (TRH_KCnsa, Fig. 12c) is very similar to model TRH_KC, with the only difference being in the amplitude of the low-velocity region under North America. However, the fast anomaly under the South Sandwich Island region still remains after the exclusion of these specific paths.

Note that the low velocities obtained southeast of South America and adjacent to high velocities in the southernmost Atlantic, are consistently present in Figs 12(a) and (c), and in good agreement with the PcP - P residuals map in Fig. 5. They do not depend on the inclusion of the very anomalous South Atlantic to Alaska paths. In Fig. 12(b), on the other hand, the same pattern is still visible, but with a somewhat weaker amplitude. Only the low velocities under the Canadian Shield are clearly dependent on the inclusion of South Atlantic to Alaska paths. Fig. 5 does seem to indicate, however, that PcP - P senses some low velocities, where there is coverage.

Using our irregular-size cell algorithm, we inverted the PKP (AB-DF) data set without the polar paths, with and without including PcP - P data and obtained very similar models as in the regular block size inversion (coefficients of correlation of 0.94 and 0.94, respectively).

Fits to the data

Fig. 13(a) shows variance reduction in PKP (AB-DF) data as a function of varying damping factors, by combining KH2001m with various D'' models as defined in Table 2. There is a direct trade-off between variance reduction and the level of P -velocity heterogeneity in D'' . As the damping factor grows, the percentage of blocks with P -velocity perturbation exceeding ± 1 per cent drops, as illustrated in Fig. 13(b). It can be seen that the TRH_KC model at optimal damping has ≈ 15 per cent of the blocks exceeding ± 1 per cent. The value of the maximum amplitude of anomalies for optimal damping in the TRH_KC model is ± 2.2 per cent. Without other geophysical constraints on the strength of heterogeneity in the lowermost mantle, it is very difficult to estimate the appropriate damping to be applied from these curves. However, we can use our PKP (BC-DF) data set, not used in the inversion process, to constrain damping, by estimating which value of damping provides the model which best fits this data set.

In Fig. 14, we show variance reductions, as a function of the damping parameter chosen, for the complete PKP (BC-DF) data set, calculated by combining predictions from D'' models (Table 2) with KH2001m. Fig. 14 shows that the best fits to the complete

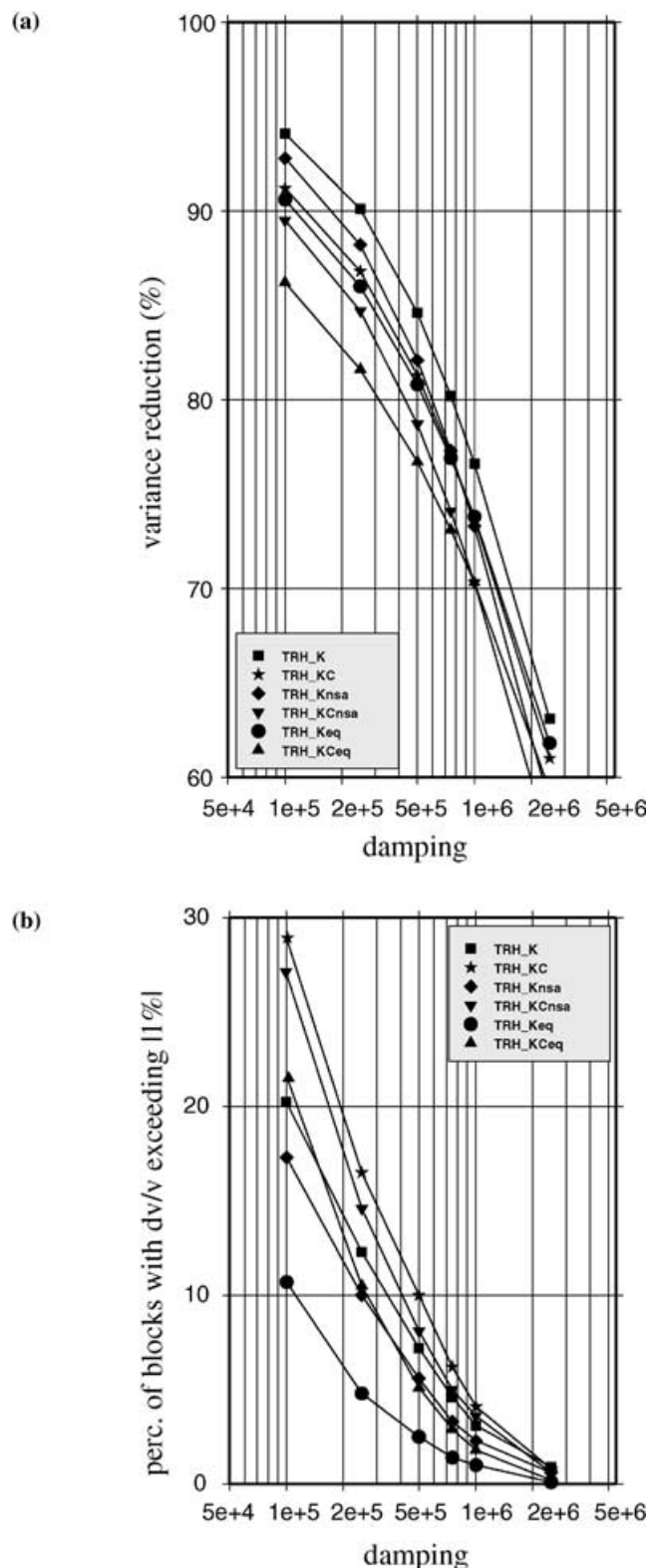


Figure 13. (a) Variance reduction in various PKP (AB-DF) data sets from Table 2 calculated from corresponding models of the lowermost 300 km of the mantle (indicated by different symbols in figure as explained in the legend), plotted as a function of damping parameter. Residuals are corrected for the KH2001m model above the lowermost 300 km of the mantle. Appropriate weighting is applied for the paths with similar geometry in calculating variance reduction, as explained in the text; (b) the percentage of blocks with perturbations exceeding ± 1 per cent for the same models as in (a).

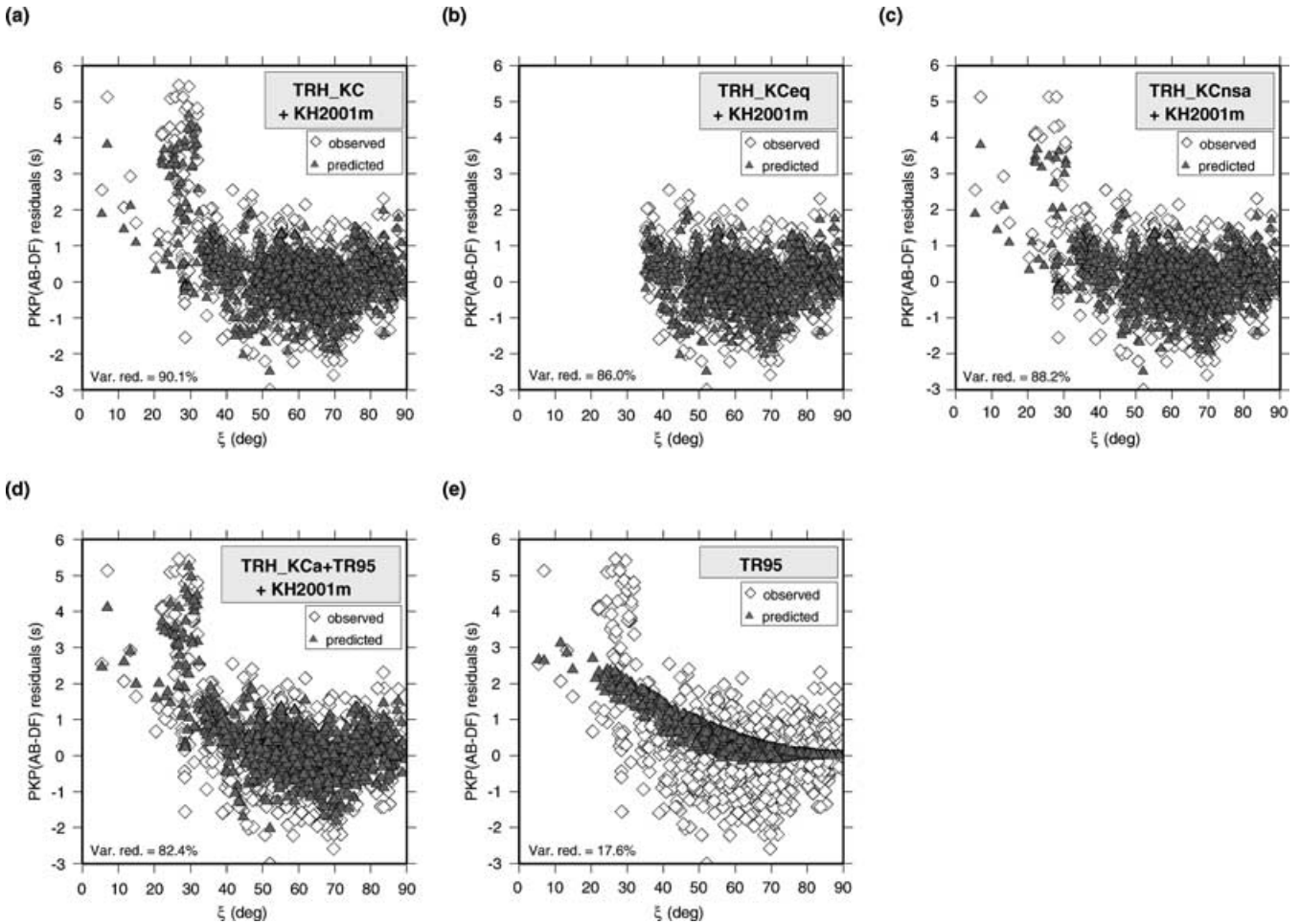


Figure 15. Observed versus predicted $PKP(AB-DF)$ residuals, plotted as a function of ξ for: (a) TRH_KC; (b) TRH_KCeq; (c) TRH_KCnsa; (d) TRH_KCa; (e) The inner-core anisotropy model TR95 used in the derivation of TRH_KCa. The predictions include the contribution of KH2001m. In (d), the predictions also include the contribution of TR95 shown in (e).

$PKP(BC-DF)$ data set are achieved for the models constructed using the complete $PKP(AB-DF)$ data set, and that an optimum damping parameter around $2.5-5 \times 10^5$ is clearly defined. This damping parameter is chosen for the final model TRH_KC shown in Figs 10(a) and 11(a). Models TRH_K and TRH_KC provide the best fit and explain about 27 per cent of the variance in $PKP(BC-DF)$. Given how close the BC and DF legs are in D'' , for any given path, it is remarkable that such a large portion of the variance in $PKP(BC-DF)$ can be explained by our relatively coarsely parametrized models.

Next, we examine observed and predicted residuals for models obtained using $PKP(AB-DF)$ and $PcP-P$ data, and the respective optimal damping parameters. We show a comparison of the observed and predicted residuals as a function of the angle ξ for TRH_KC, TRH_KCeq and TRH_KCnsa in Figs 15(a)–(c), respectively. The cluster of very large observed residuals that is not completely explained by our models corresponds to very specific paths from the South Atlantic to Alaska and the South Atlantic to northern Asia (mostly for the event in the South Atlantic mentioned earlier). However, between $\xi = 20^\circ$ and 45° , model TRH_KC is able to explain a range of 6 s. It also successfully explains the larger scatter of ‘equatorial’ data as opposed to ‘polar’ data. Fig. 15(d) shows the predictions of model TRH_KCa combined with the corresponding inner-core anisotropy model and with KH2001a. Fig. 15(e) shows,

for reference the predictions of the inner-core anisotropy model alone. The variance reduction in the $PKP(AB-DF)$ data set is only 17.6 per cent when only inner-core anisotropy is considered, and the distribution of the predictions does not match that of the data. Combining inner-core anisotropy with TRH_KCa and KH2001m, we obtain a variance reduction of 82.4 per cent, a value that is slightly less than for model TRH_KC (with KH2001m, Fig. 15a). However, some polar data at angles $\xi < 30^\circ$ are explained slightly better.

Figs 16(a)–(c) show the predictions for $PcP-P$ residuals, obtained using model KH2001m, combined with models TRH_KC, TRH_KCeq and TRH_KCnsa, respectively. More than 50 per cent of the variance in $PcP-P$ can be explained by any of the models, which indicates that:

- (1) a significant portion of the variance in $PcP-P$ is attributable to D'' , as previously inferred from Fig. 7; and
- (2) the inclusion of polar paths is not incompatible with the constraints from $PcP-P$.

Finally, we analyse the fits to the $PKP(BC-DF)$ data set obtained for the different models. Fig. 17(a) shows the $PKP(BC-DF)$ observed and predicted residuals as a function of ξ for model TRH_KC (with KH2001m). The scatter in equatorial paths is well explained, however, this model does not explain the large residuals for polar paths. Fig. 17(b) shows the predictions of the inner-core anisotropy

model alone. This model does not explain the scatter in the equatorial data, but it explains the larger residuals on polar paths better, resulting in an overall variance reduction of 44.2 per cent, compared with only 27 per cent for model TRH_KC. The combination of the inner-core anisotropy model, corresponding to the D'' model TRH_KCa and KH2001m results in a slight improvement in variance reduction (54.5 per cent, Fig. 17c). Adding the D'' model helps to explain more of the scatter on equatorial paths. However, a large portion of the most anomalous data near $\xi = 30^\circ$ still remains unexplained (at least 2 s).

6 DISCUSSION AND CONCLUSIONS

We inverted a large data set of hand-picked $PKP(AB-DF)$ and $PcP-P$ traveltime data to retrieve the P -velocity structure of the lowermost 300 km of the mantle, after correcting for overlying mantle structure, using the tomographic P model, stripped of the last 300 km of the mantle, which provides the best fit to both data sets (KH2001m). We demonstrated that the exclusion or inclusion of polar paths does not change the derived P -velocity model of D'' significantly, except in areas where coverage is provided only when polar paths are included (mostly for North America).

Our results demonstrate that, with a significant number of high-quality PKP differential traveltime data, we are able to retrieve

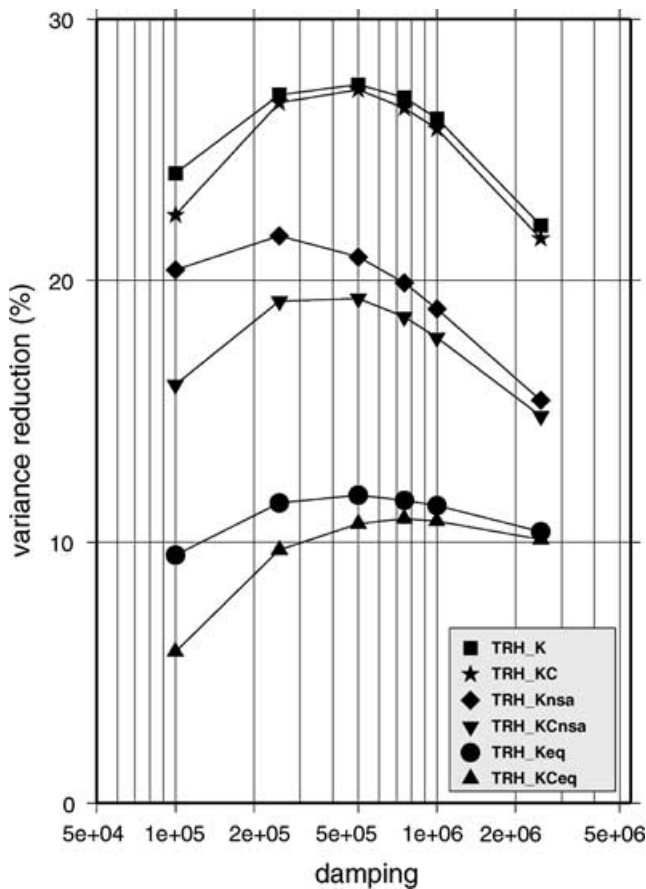


Figure 14. Variance reduction in the complete $PKP(BC-DF)$ data set obtained for models TRH_K and TRH_KC (indicated by different symbols in figure), plotted as a function of damping parameter. Residuals are corrected for the KH2001m model above the lowermost 300 km of the mantle. Appropriate weighting is applied for the paths with similar geometry in calculating variance reduction as explained in the text.

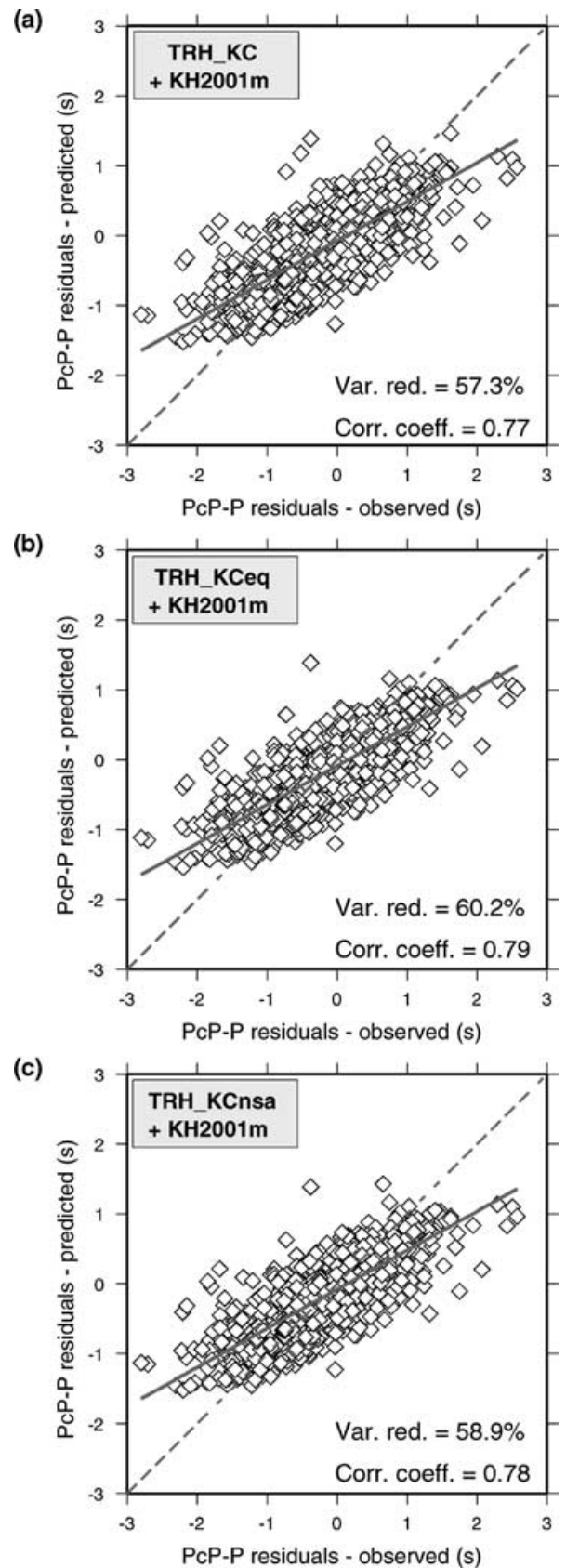


Figure 16. Observed versus predicted $PcP-P$ residuals for: (a) TRH_KC; (b) TRH_KCeq; (c) TRH_KCnsa. The predictions include the contribution of KH2001m. Variance reduction and correlation coefficients are indicated. Solid line is the best linear fit.

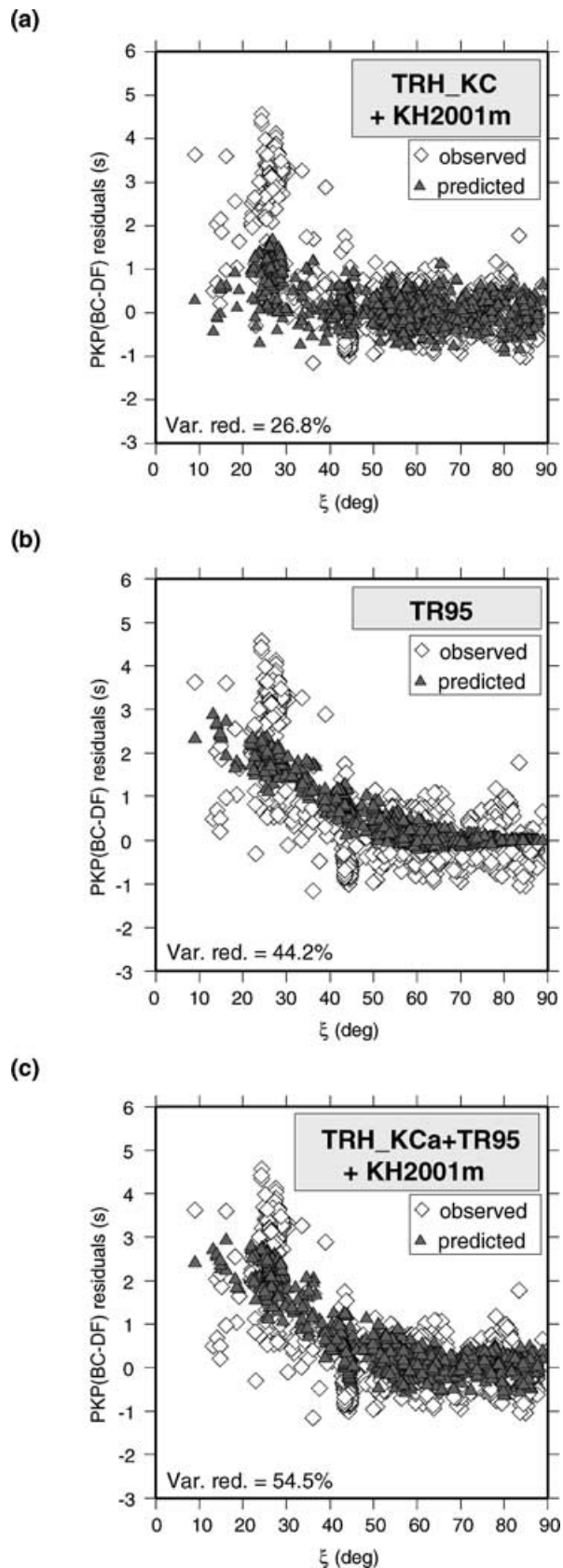


Figure 17. Observed (diamonds) versus predicted (triangles) $PKP(BC-DF)$ residuals as a function of ξ for: (a) model TRH_KC combined with KH2001m; (b) radial model of inner-core anisotropy (TR95); (c) model TRH_KCa, combined with KH2001m and TR95.

D'' maps that are compatible with maps obtained using independent body-wave data sets. The combination of our preferred D'' model and KH2001m can explain over 80 per cent of the variance in $PKP(AB-DF)$ and over 50 per cent of the variance in $PcP-P$, as well as a significant portion of the variance in our $PKP(BC-DF)$ data set (close to 30 per cent), not used in the inversion.

We showed that accounting for a radial model of inner-core anisotropy, compatible with normal mode splitting data, prior to inversion, produces a model of D'' that is very similar to the models for which inner-core anisotropy is not included, although with smaller amplitudes of lateral variations. Such a model, combined with KH2001m, results in better predictions of $PKP(BC-DF)$, but degrades slightly the predictions of $PKP(AB-DF)$ residuals. There remains a significant portion of the $PKP(BC-DF)$ residuals on anomalous paths between the South Atlantic and Alaska, which this type of model, combining simple, axisymmetric anisotropy in the inner core and D'' heterogeneity at intermediate wavelengths, cannot explain.

In areas of good coverage, our models TRH_KC and TRH_KCa provide stable and reliable maps of lateral variations of velocity in D'' at a scalelength of several hundred kilometres. The next step is, on the one hand, to improve the coverage by incorporating other hand independent data such as $Pdiff-PKP$ at appropriate distance ranges, and, on the other hand, to examine short-scale variations in D'' structure as can be addressed using dense arrays such as that in Alaska. This will be addressed in forthcoming contributions.

In the present study, we have also ignored possible contributions from core–mantle boundary topography, which could possibly further improve the fits to our data sets (e.g. Creager & Jordan 1986; Morelli *et al.* 1986; Rodgers & Wahr 1993; Obayashi & Fukao 1997).

ACKNOWLEDGMENTS

We thank two anonymous reviewers who helped us to improve the manuscript. We are grateful to Ludovic Bréger for his helpful comments, and numerous colleagues at UC Berkeley for their suggestions. We thank Ken Creager, Tom McSweeney, Annie Souriau, Satoru Tanaka and Michael Wyession, for generously providing their data, and also to Roger Hansen, Kent Lindquist, Doug Christensen and personnel of UAF Geophysical Institute, Bill Shannon, Sylvia Lehman and Luc Saumure from CNSN, and Fumiko Tajima from UCB. Many thanks to IRIS, Geoscope, GRSN, Mednet and BDSN teams. Figures were made with the General Mapping Tools (P. Wessel & W. H. F. Smith, 1995 *EOS, Trans. Am. geophys. Un.*, **76**, 329). This work was supported by NSF grant no EAR-9902777 and IGPP/LLNL grant no 00-GS-010. It is BSL contribution 01-05.

REFERENCES

- Bataille, K. & Flatte, S.M., 1988. Inhomogeneities near the core–mantle boundary inferred from short-period scattered PKP waves recorded at the GDSN, *J. geophys. Res.*, **93**, 15 057–15 064.
- Bijwaard, H., Spakman, W. & Engdahl, R., 1998. Closing the gap between regional and global traveltome tomography, *J. geophys. Res.*, **103**, 30 055–30 078.
- Boschi, L.J. & Dziewonski, A.M., 2000. Whole Earth tomography from delay times of P , PcP , PKP phases: lateral heterogeneities in the outer core, or radial anisotropy in the mantle?, *J. geophys. Res.*, **105**, 13 675–13 676.
- Bréger, L. & Romanowicz, B., 1998. Three-dimensional structure at the base of the mantle beneath the central Pacific, *Science*, **282**, 718–720.

- Bréger, L., Tkalčić, H. & Romanowicz, B., 2000. The effect of D'' on PKP(AB–DF) travel time residuals and possible implications for inner core structure, *Earth planet. Sci. Lett.*, **175**, 133–143.
- Castle, J.C. & van der Hilst, R.D., 2000. The core–mantle boundary under the Gulf of Alaska: no ULVZ for shear waves, *Earth planet. Sci. Lett.*, **176**, 311–321.
- Cornier, V.F. & Choy, G.L., 1986. A search for lateral heterogeneity in the inner core from differential travel times near PKP–D and PKP–C, *Geophys. Res. Lett.*, **13**, 1553–1556.
- Creager, K.C., 1992. Anisotropy of the inner core from differential travel times of the phases PKP and PKIKP, *Nature*, **356**, 309–314.
- Creager, K.C., 1999. Large-scale variations in inner core anisotropy, *J. geophys. Res.*, **104**, 23 127–23 139.
- Creager, K.C. & Jordan, T.H., 1986. Aspherical structure of the core–mantle boundary from PKP travel times, *Geophys. Res. Lett.*, **13**, 1497–1500.
- Doornbos, D.J., 1974. Seismic wave scattering near caustics: observation of PKKP precursors, *Nature*, **247**, 34–35.
- Durek, J. & Romanowicz, B., 1999. Inner core anisotropy inferred by direct inversion of normal mode spectra, *Geophys. J. Int.*, **139**, 599–622.
- Engdahl, E.R., van der Hilst, R.D. & Buland, R.P., 1998. Global teleseismic earthquake relocation with improved travel times and procedures for depth determination, *Bull. seism. Soc. Am.*, **88**, 722–743.
- Grand, S.P., van der Hilst, R.D. & Widiyantoro, S., 1997. Global seismic tomography: a snapshot of convection in the Earth, *GSA Today*, **7**, 1–7.
- Garcia, R. & Souriau, A., 2000. Amplitude of the core mantle boundary topography estimated by stochastic analysis of core phases, *Phys. Earth planet. Inter.*, **117**, 345–359.
- Garnero, E.J., 2000. Heterogeneity of the lowermost mantle, *Ann. Rev. Earth planet. Sci.*, **28**, 509–537.
- Garnero, E.J. & Helmberger, D.V., 1995. A very slow basal layer underlying large-scale low velocity anomalies in the lower mantle beneath the Pacific: evidence from core phases, *Phys. Earth planet. Inter.*, **91**, 161–176.
- Garnero, E.J. & Helmberger, D.V., 1996. Seismic detection of a thin laterally varying boundary layer at the base of the mantle beneath the central-pacific, *Geophys. Res. Lett.*, **23**, 977–980.
- Garnero, E.J., Ravenaugh, J.S., Williams, Q., Lay, T. & Kellogg, L.H., 1998. Ultralow velocity zone at the core–mantle boundary, in *The Core–Mantle Boundary*, pp. 319–334, eds Gurnis, M., Wysession, M.E., Knittle, E. & Buffet, B.A., AGU, Washington, DC.
- Gu, Y. & Dziewonski, A.M., 2000. Shear velocity of the mantle and discontinuities in the pattern of lateral heterogeneities, *J. geophys. Res.*, **106**, 11 169–11 199.
- Haddon, R.A.W. & Cleary, J.R., 1974. Evidence for scattering of seismic PKP waves near the mantle–core boundary, *Phys. Earth planet. Inter.*, **8**, 211–234.
- Husebye, E.S., King, D.W. & Haddon, R.A.W., 1976. Precursors to PKIKP and seismic wave scattering near the mantle–core boundary, *J. geophys. Res.*, **81**, 1870–1882.
- Kárasón, H. & van der Hilst, R.D., 2001. Improving global tomography models of P -wavespeed I: incorporation of differential times for refracted and diffracted core phases (PKP, P_{diff}), *J. geophys. Res.*, **106**, 6569–6587.
- Kennett, B.L.N., Engdahl, E.R. & Buland, R., 1995. Constrains on seismic velocities in the Earth from traveltimes, *Geophys. J. Int.*, **122**, 108–124.
- Kuo, B.-Y., 1999. Amplitude of S_{diff} across Asia: effects of velocity gradient and Q_s in the D'' region and the asphericity of the mantle, *Earth planet. Sci. Lett.*, **173**, 101–112.
- Li, X.-D. & Romanowicz, B., 1996. Global mantle shear-velocity model developed using nonlinear asymptotic coupling theory, *J. geophys. Res.*, **101**, 22 245–22 272.
- Masters, G., Johnson, S., Laske, G. & Bolton, B., 1996. A shear-velocity model of the mantle, *Phil. Trans. R. Soc. Lond., A*, **354**, 1385–1411.
- Masters, G., Bolton, H. & Laske, G., 1999. Joint seismic tomography for P and S velocities: how pervasive are chemical anomalies in the mantle?, *EOS, Trans. Am. geophys. Un.*, **80**, S14.
- McSweeney, T.J., Creager, K.C. & Merrill, R.T., 1997. Depth extent of inner-core seismic anisotropy and implications for geomagnetism, *Phys. Earth planet. Inter.*, **101**, 131–156.
- Mégnin, C. & Romanowicz, B., 2000. The 3D shear velocity structure of the mantle from the inversion of body, surface, and higher mode waveforms, *Geophys. J. Int.*, **143**, 709–728.
- Morelli, A., Dziewonski, A.M. & Woodhouse, J.H., 1986. Anisotropy of the core inferred from PKIKP travel times, *Geophys. Res. Lett.*, **13**, 1545–1548.
- Ni, S. & Helmberger, D.V., 2000. Horizontal transition from fast (slab) to slow (plume) structures at the core–mantle boundary, *Earth planet. Sci. Lett.*, **187**, 310.
- Obayashi, M. & Fukao, Y., 1997. P and PcP travel time tomography for the core–mantle boundary, *J. geophys. Res.*, **102**, 17 825–17 841.
- Press, W.H., Flannery, B.P., Teukolsky, S.A. & Vetterling, W.T., 1988. *Numerical Recipes in C*, Cambridge University Press, Cambridge.
- Ritsema, J., Ni, S., Helmberger, D.V. & Crotwell, H.P., 1998. Evidence for strong shear velocity reductions and velocity gradients in the lower mantle beneath Africa, *Geophys. Res. Lett.*, **25**, 4245–4248.
- Rodgers, A. & Wahr, J., 1993. Inference of core–mantle boundary topography from ISC PcP and PKP travel times, *Geophys. J. Int.*, **115**, 991–1011.
- Romanowicz, B. & Bréger, L., 2000. Anomalous splitting of free oscillations: a reevaluation of possible interpretations, *J. geophys. Res.*, **105**, 21 559–21 578.
- Romanowicz, B., Tkalčić, H. & Bréger, L., 2001. On the origin of complexity in PKP travel time data from broad-band records, in *AGU Volume on Inner Core and Lower Mantle, AGU Geodynamic Series*, ed. Dehant, V., in revision.
- Sacks, I.S., Snoke, J.A. & Beach, L., 1979. Lateral heterogeneity at the base of the mantle revealed by observations of amplitudes of PKP phases, *Geophys. J. R. astr. Soc.*, **59**, 379–387.
- Snocke, J.A. & Sacks, I.S., 1986. Seismic modeling of lateral heterogeneity at the base of the mantle, *Geophys. J. R. astr. Soc.*, **86**, 801–814.
- Souriau, A. & Poupinet, G., 1994. Lateral variations in P velocity and attenuation in the D'' layer, from diffracted P waves, *Phys. Earth planet. Inter.*, **84**, 227–234.
- Souriau, A. & Romanowicz, B., 1996. Anisotropy in inner core attenuation: a new type of data to constrain the nature of the solid core, *Geophys. Res. Lett.*, **23**, 1–4.
- Su, W.-J., Woodward, R.L. & Dziewonski, A.M., 1994. Degree 12 model of shear velocity heterogeneity in the mantle, *J. geophys. Res.*, **99**, 6945–6980.
- Sylvander, M. & Souriau, A., 1996. P -velocity structure of the core–mantle boundary region inferred from PKP(AB)–PKP(BC) differential travel times, *Geophys. Res. Lett.*, **23**, 853–856.
- Sylvander, M., Ponce, B. & Souriau, A., 1997. Seismic velocities at the core–mantle boundary inferred from P waves diffracted around the core, *Phys. Earth planet. Inter.*, **101**, 189–202.
- Tanaka, S. & Hamaguchi, H., 1997. Degree one heterogeneity and hemispherical variation of anisotropy in the inner core from PKP(BC)–PKP(DF) times, *J. geophys. Res.*, **102**, 2925–2938.
- Tkalčić, H., Romanowicz, B. & Houy, N., 2001. Constraints on $d \ln V_s / d \ln V_p$ from high-quality broad-band records, in preparation.
- Tkalčić, H. & Romanowicz, B., 2002. Short scale heterogeneity in the lowermost mantle: insights from PcP – P and ScS – S data, *Earth planet. Sci. Lett.*, in press.
- Tromp, J., 1993. Support for anisotropy of the Earth's inner core from free oscillations, *Nature*, **366**, 678–681.
- Tromp, J., 1995. Normal-mode splitting observations from the great 1994 Bolivia and Kuril Island earthquakes: constraints on the structure of the mantle and inner core, *GSA Today*, **5**, 137–151.
- van der Hilst, R.D., Widiyantoro, S. & Engdahl, E.R., 1997. Evidence of deep mantle circulation from global tomography, *Nature*, **386**, 578–584.
- Vasco, D.W. & Johnson, L.R., 1998. Whole earth structure estimated from seismic arrival times, *J. geophys. Res.*, **103**, 2633–2671.
- Williams, Q. & Garnero, E.J., 1996. Seismic evidence for partial melt at the base of Earth's mantle, *Science*, **273**, 1528–1530.
- Woodhouse, J.H., Giardini, D. & Li, X.-D., 1986. Evidence for inner core anisotropy from splitting in free oscillation data, *Geophys. Res. Lett.*, **13**, 1549–1552.

Wysession, M.E., Okal, E.A. & Bina, C.R., 1992. The structure of the core–mantle boundary from diffracted waves, *J. geophys. Res.*, **97**, 8749–8764.

Wysession, M.E., Valenzuela, R.W., Zhu, A. & Bartko, L., 1995. Investigating the base of the mantle using differential travel times, *Phys. Earth planet. Inter.*, **92**, 67–84.

Wysession, M.E., 1996. Large-scale structure at the core–mantle boundary from diffracted waves, *Nature*, **382**, 244–248.

Wysession, M.E., Fischer, K.M., Al-eqabi, G.I. & Shore, P.J., 2000. Using MOMA broad-band array, *ScS*–*S* data to image smaller-scale structures at the base of the mantle, *Geophys. Res. Lett.*, **28**, 867–870.